Large-eddy simulation of turbulent gas–particle flow in a vertical channel: effect of considering inter-particle collisions

By Y. YAMAMOTO†, M. POTTHOFF‡, T. TANAKA¶,
T. KAJISHIMA AND Y. TSUJI

Department of Mechanical Engineering, Osaka University, Yamada-oka 2-1, Suita, Osaka,
565-0871 Japan

The interaction between a turbulent gas flow and particle motion was investigated by numerical simulations of gas–particle turbulent downward flow in a vertical channel. In particular the effect of inter-particle collision on the two-phase flow field was investigated. The gas flow field was obtained by large-eddy simulation (LES). Particles were treated by a Lagrangian method, with inter-particle collisions calculated by a deterministic method. The spatial resolution for LES of gas–solid two-phase turbulent flow was examined and relations between grid resolution and Stokes number are presented. Profiles of particle mean velocity, particle wall-normal fluctuation velocity and number density are flattened as a result of inter-particle collisions and these results are in good agreement with experimental measurements. Calculated turbulence attenuation by particles agrees well with experimental measurements for small Stokes numbers, but not for large Stokes number particle. The shape and scale of particle concentrations calculated considering inter-particle collision are in good agreement with experimental observations.

1. Introduction

One of the most interesting problems in fluid dynamics is the prediction of particle-laden turbulent flows. This kind of flow occurs in many technical processes in chemical engineering, mineral processing, energy conversion and air pollution control. In such processes, the fluid flow is turbulent, and turbulence plays a very important role in transport of mass, momentum and energy between the solid and fluid phases. Modification of turbulence characteristics by solid particles has been shown by various experiments (see Gore & Crowe 1991). This turbulence modification is a very interesting physical phenomenon. For engineering applications, the interest is in how the effect of particles should be modelled in codes for two-phase flow analysis.

1.1. *Experimental work*

A review of experimental work on turbulence modification by particles is given by Gore & Crowe (1991). They reviewed available experimental data of gas/solid,

† Present address: Department of Industrial Engineering, Kansai University, Yamate-cho 3-3-35, Suita, Osaka, 564-8680 Japan.
‡ Present address: Fertilizer and Inorganic Acid Division, UHDE GmbH, 44141 Dortmund, Germany.
¶ Author to whom correspondence should be addressed.

gas/liquid, liquid/solid and liquid/gas systems in pipes and jets and concluded that the ratio of particle diameter and turbulence length scale is an appropriate measure to decide if the turbulence intensity of the carrier fluid is augmented or attenuated by dispersed particles: if this ratio is larger than 0.1 it increases, otherwise it decreases. However, the data are scattered and indications about the degree of increase or decrease versus flow condition are not provided.

The Stokes number St is another parameter often used to represent the influence of particles on fluid turbulence:

$$St = \frac{\tau_p}{\tau_f}, \tag{1.1}$$

where τ_p is particle relaxation time and τ_f is the characteristic time scale of fluid turbulence. When the Stokes number is 0, particles completely follow the fluid motion as ideal tracers, while at very large Stokes number particles move independently of turbulent eddies.

To understand the degree of attenuation of fluid turbulence intensity by solid particles, Kulick, Fessler & Eaton (1994) did measurements in a vertical downward channel flow in which small, dense particles were dispersed uniformly. The flow was fully developed and the maximum mass loading was 0.8. They measured profiles of the mean and fluctuating velocity of particles and gas for varying Stokes number and mass loading ratio. They found that (i) the profile of particle mean velocity is flat due to diffusion in the wall-normal direction, (ii) r.m.s. streamwise particle fluctuation velocity is larger than the streamwise turbulence intensity of the gas, while the r.m.s. wall-normal component is less than the wall-normal turbulence intensity, (iii) the degree of turbulence attenuation increases with Stokes number and mass loading, and (iv) power spectrum of gas velocity fluctuations increases in strength in the high-frequency region and is suppressed in the low-frequency region by the effect of particles.

For modelling of the effect of particles on fluid turbulence, information on particle motion in two-phase flows is essential. The structure of particle distribution and turbulence in the near-wall region was observed by Rashidi, Hetsroni & Banerjee (1990) and Kaftori, Hetsroni & Banerjee (1995a, b) using oxygen bubble visualization for the particle-laden open channel flow of water. They found that particles are affected by coherent wall structures and tend to form streaky structure in regions of low fluid velocity. The particle distribution in the channel centreplane was observed by Fessler, Kulick & Eaton (1994) using a laser sheet in the same facility as Kulick *et al*. They found that particles of small Stokes number are preferentially concentrated, and the degree of preferential concentration is large when the Stokes number based on the Kolmogorov time scale approaches 1.

1.2. *Previous simulations*

In recent years direct numerical simulation (DNS) and large-eddy simulation (LES) have become powerful tools for the study of two-phase flow. Squires & Eaton (1990) and Elghobashi & Truesdell (1992, 1993) performed DNS of unbounded, homogeneous and isotropic turbulence considering fluid/particle and particle/fluid interactions (so called two-way coupling). Concerning turbulence modification Squires & Eaton (1990) concluded that heavier particles, which are more uniformly dispersed in turbulence, cause a more homogeneous modification of turbulence properties than lighter ones. Light particles tend to accumulate in regions of high strain rate and low vorticity while heavy particles are much less influenced by the fluid motion. Their

results show further that the additional source term in the momentum equation of the fluid arising from coupling of particles with the fluid acts as a sink for turbulence kinetic energy. Dissipation of turbulence energy is increased by the presence of small solid particles and increases with solid volume fraction. Elghobashi & Truesdell (1992, 1993) solved the full equation for particle motion including gravity and Basset history terms and showed that gravity acts as a permanent source of energy to the turbulence. Particle dispersion is strongly affected by gravity and turbulence modification occurs: particles transfer gravitational potential energy to the high-wavenumber motions in the gravity direction. This anisotropy is then removed by transfer of energy into the two horizontal directions, leading to a reverse cascade. This leads to an energy transfer into the low-wavenumber region and a reduced decay rate compared with particle-free turbulence.

The structure of particle distribution and turbulence in the near-wall region of a horizontal water channel was examined by Pedinotti, Mariotti & Banerjee (1992) using one-way coupled DNS, and Pan & Banerjee (1996, 1997) using two-way coupled DNS. Pedinotti *et al.* showed that particles are affected by the quasi-streamwise vortices and tend to concentrate in low-speed streaks. Pan & Banerjee (1996, 1997) showed that particles accumulate in the low-speed streaks and the ejection–sweep cycle is affected by particles. They used new models for the effect of particles in the fluid-phase calculation to obtain the flow field around a particle in detail. Their models require too much computational time to calculate a large number of particles. Rouson & Eaton (1994) performed a one-way coupled DNS of downward gas–solid channel flow with similar conditions to the experiments by Kulick *et al.*, but where the Reynolds number ($Re = 1860$) was much less than that of the experiments ($Re = 13\,800$). They showed snapshots of particle distributions in the near-wall region, and concluded that large-inertia particles tend to disperse uniformly while small-inertia particle tend to accumulate in low-speed streaks and to form particle clouds. They indicated some qualitative agreement between the statistical quantities of the experiments and the simulation, but not quantitative agreement.

These DNS simulations were done at rather low Reynolds numbers because of the huge computer capacity required for simulations of high Reynolds number flow. Wang & Squires (1996) performed a one-way coupled LES of particle-laden turbulent channel flow for the same conditions as those of the experiments by Kulick *et al.* and Fessler *et al.* and the DNS by Rouson & Eaton. Their computed particle distribution showed the same trends as the numerical results by Rouson & Eaton in the near-wall region, and as Fessler *et al.* in the channel-centre region. However, the shape of particle clouds in the channel-centre region was longer in the streamwise direction, which is different from the experimental observations by Fessler *et al.* This discrepancy was considered to be due to the effect of inter-particle collision.

1.3. *Inter-particle collision*

In the above-mentioned simulations, inter-particle collisions are neglected. Tanaka & Tsuji (1991) performed a one-way coupled simulation of gas–solid flow with an assumed gas-phase velocity and accounting for inter-particle collisions. They found that the effect of inter-particle collisions on the diffusion in the direction normal to the mean flow cannot be neglected even in conditions generally considered to be dilute (solid volume fraction is $O(10^{-4})$). They treated inter-particle collision using the technique of uncoupling (Bird 1976) with inter-particle collisions calculated by a deterministic method.

Methods of calculation of inter-particle collision include the deterministic method,

stochastic method, continuous model, etc. Sommerfeld (1995) performed a one-way coupled simulation of gas-solid flow in a horizontal channel and demonstrated the importance of inter-particle collisions. In his method, the occurrence of collisions is treated stochastically through a local probability of collision. Such a statistical treatment requires that the particle number density is sufficiently high. Simonin (1991) proposed a two-fluid model with the effect of inter-particle collision derived by analogy with molecular dynamics. In his simulation, their effect is modelled as a diffusion coefficient. However, friction between particles is not considered and non-elastic collision cannot be treated. Furthermore the constitutive equation is very complicated and includes many assumptions. Yonemura, Tanaka & Tsuji (1993) performed a two-way coupled simulation of gas–solid flow accounting for inelastic inter-particle collisions. They found that particle clouds are formed by the effect of such collisions and that the large-scale gas flow is affected by the particle clouds. They used the direct simulation Monte Carlo (DSMC) method (Bird 1976) which is used in the field of rarefied gas simulations. A stochastic method assumes that the flow field in a calculation cell is homogeneous. Therefore the method cannot be applied to flows that have large velocity gradients such as turbulent channel flow. Furthermore, the gas flow was assumed to be inviscid so that the interaction between particles and turbulence was neglected.

Concerning turbulence simulation considering the effect of inter-particle collision, there is some work on collision frequency in isotropic turbulence by one-way coupled DNS (Wang, Wexler & Zhou 1998*a*,*b*; Sundaram & Collins 1997). Sundaram & Collins (1999) performed two-way coupled DNS of isotropic turbulence including the effect of inter-particle collision to study turbulence modulation. They found that the rate of viscous dissipation of turbulent energy is enhanced by particles. But the differences of the flow fields with and without the effect of inter-particle collision were not examined.

1.4. *Objectives and outline*

In this study, the interaction between particle motion and gas turbulence is examined by numerical simulation. We chose to study the flow between two parallel walls because many simulations of single-phase turbulent flow have been performed of this flow, and in particular vertical downward channel flow so as to compare the results with experimental data by Kulick *et al.* (1994) and Fessler *et al.* (1994).

To study the high Reynolds number flow produced experimentally by Kulick *et al.* and Fessler *et al.*, we calculated the gas flow by LES with two-way coupling in order to consider the effect of particle motion on the gas phase. For the solid-phase calculation, individual particles were tracked by a Lagrangian method and inter-particle collisions were taken into account. Inter-particle collision was treated by the techniques of uncoupling and deterministic collision prediction in the same way as Tanaka & Tsuji (1991). Through this technique, statistical properties and instantaneous fields were analysed and compared with experimental results to study the interaction between particle motion and gas turbulence. In particular, the effect of inter-particle collision on the flow field was clarified. Furthermore, the required spatial resolution for two-phase LES was also examined.

2. Simulation procedure

The simulations were performed under conditions chosen to match the experiments by Kulick *et al.* (1994) and Fessler *et al.* (1994). Figure 1 shows the calculation
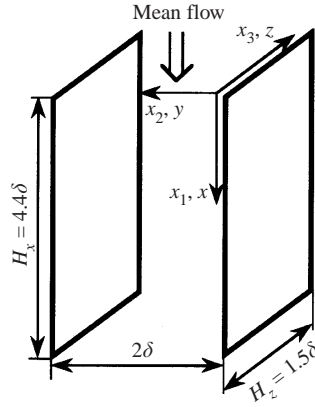
FIGURE 1. Calculation configuration.

configuration. Periodic boundary conditions were applied in the streamwise (x) and spanwise (z) directions due to restrictions on computational power. The channel half-width is $\delta = 0.02$ m, the length of the calculation region in the streamwise direction $H_x = 4.4\delta$ and $H_z = 1.5\delta$ in the spanwise direction. The size of computational domain employed in this study is smaller than the other reseachers' DNS or LES because of limited computational capacity. Two-point correlations of velocity components in the streamwise and spanwise direction were calculated (the results were omitted from this paper). The convergence of correlations was not good enough, so there is not complete statistical independence associated with the periodic boundary. But, numerical results of turbulence statistics were in good agreement with experimental measurements, and the size of the structure of particle distribution caused by turbulence was much smaller than the domain size, so we considered that it is possible to study the effect of inter-particle collision which is the main issue in this study.

The fluid is air (kinematic viscosity as $v = 1.5 \times 10^{-5}$ m^2 s^{-1}), and the friction velocity u_τ is 0.49 m s^{-1}. The Reynolds number Re_τ based on channel half-width δ and friction velocity u_τ is 644.

The flow is driven by a constant pressure gradient. Considering the macroscopic momentum balance in the computational domain, we find

$$2\delta H_z[\overline{(p + \Delta p)} - \bar{p}] = -2H_x H_z \tau_w + N m_p g,$$

in which, $\tau_w = \rho u_\tau^2$ is mean wall shear stress, N is the number of particles in the calculation region and an overbar denotes the average value. The mean pressure gradient is given by

$$\frac{\overline{\Delta p}}{H_x} = -\frac{\rho u_\tau^2}{\delta} + \frac{N m_p g}{2 H_x \delta H_z}. \tag{2.1}$$

The procedure of two-way coupling is as follows. In each step, particle motion is calculated first: all aerodynamic forces on a particle are calculated by using the fluid velocity at the particle point explicitly. After all particle motions are calculated, the volumetric-averaged aerodynamic force on each fluid computational cell is calculated, and fluid motion is calculated using the volumetric-averaged aerodynamic force explicitly.

2.1. *Fluid motion*

To calculate the fluid flow field, large-eddy simulation (LES) was performed. In LES the fluid flow field is divided into a large-scale motion resolved by the computation and small-scale, 'sub-grid scale' (SGS) fluctuation by 'filtering'. The large-scale flow field is calculated taking into account the effects of SGS fluctuations according to the following equations:

$$\frac{\partial u_i}{\partial x_i} = 0, \tag{2.2}$$

$$\frac{\partial u_i}{\partial t} + \frac{\partial u_i u_j}{\partial x_j} = -\frac{\partial}{\partial x_i}\left(\frac{p}{\rho} + \frac{\overline{\Delta p}}{\rho H_x}x_1\right) + \frac{\partial}{\partial x_j}2\nu S_{ij} - \frac{\partial}{\partial x_j}\overline{u_i' u_j'}^{(SGS)} + \frac{\overline{\Delta p}}{\rho H_x}\delta_{i1} + \frac{f_{pi}}{\rho},$$

$$\tag{2.3}$$

in which u_i and p are grid-scale velocity and pressure; $\boldsymbol{f}_p$ expresses the action on the fluid of the particles, given by the sum of all forces except gravity on the right-hand side of equation (2.7) in §2.2 of all particles in a fluid computational cell,

$$\boldsymbol{f}_p = -\frac{1}{V_{cell}}\sum_{j=1}^{N_{cell}}\boldsymbol{f}_{fj}, \tag{2.4}$$

where V_{cell} is the volume of a fluid computational cell, N_{cell} is the number of particles in that cell and $\boldsymbol{f}_{fj}$ is the fluid force on the jth particle in that cell (see equation (2.7)). In this study, the solid volume fraction is so low that the volume of particles is neglected in the fluid calculation. S_{ij} is the strain rate tensor, $S_{ij} = (1/2)(\partial u_i/\partial x_j + \partial u_j/\partial x_i)$, and $\overline{u_i' u_j'}^{(SGS)}$ is SGS stress. In this work, we neglected the effect of particles on SGS stress because of lack of information. Accordingly, we applied the Smagorinsky model (Deardorff 1970) for SGS stress, the most common model used for single-phase LES, given by

$$\left.\begin{array}{l}\overline{u_i' u_j'}^{(SGS)} = -2\nu_{SGS}S_{ij} + \frac{1}{3}\delta_{ij}\overline{u_k' u_k'}^{(SGS)}, \\ \nu_{SGS} = (C_s f_s \Delta_s)^2 \left(2S_{ij}S_{ij}\right)^{1/2},\end{array}\right\} \tag{2.5}$$

where $C_s = 0.1$ is the Smagorinsky constant, Δ_s is the filter scale, given for a staggered grid by $\Delta_s = (\Delta x_1 \Delta x_2 \Delta x_3)^{1/3}$ with mesh width Δx_i. A damping function f_s is necessary because ν_{SGS} has to be zero at the wall. In LES, a Van Driest type damping function such as $f_s = 1 - \exp(-y^+/25)$ is commonly used, where y^+ is distance from the wall measured in wall units, i.e. $y^+ = yu_\tau/\nu$. The dynamic SGS model (Germano *et al.* 1991), which does not need this damping function, is most often used but it needs plane averaging to avoid the numerical instability. In the present study, local particle concentration can be high and this can cause a local change of fluid flow. If that happens, plane averaging transmits the effect of the local change to the whole field in that plane. Thus we did not consider the dynamic model suitable in this case and used Smagorinsky model. Using these models, equation (2.3) becomes

$$\frac{\partial u_i}{\partial t} + \frac{\partial u_i u_j}{\partial x_j} = -\frac{\partial P}{\partial x_i} + \frac{\partial}{\partial x_j}\left[2(\nu + \nu_{SGS})S_{ij}\right] + \frac{\overline{\Delta p}}{\rho H_x}\delta_{i1} + \frac{f_{pi}}{\rho}, \tag{2.6}$$

where

$$P = \frac{p}{\rho} + \frac{\overline{\Delta p}}{\rho H_x}x_1 + \frac{1}{3}\overline{u_k' u_k'}^{(SGS)}.$$

These equations were solved by a finite difference method, the same scheme as in the single-phase LES by Kajishima & Miyake (1990). In the streamwise and spanwise directions, uniform grids were used. In the direction normal to the wall, grid points were concentrated in the near-wall region according to a tanh function (Moin & Kim 1982). Spatial derivatives were approximated by a second-order-accurate central finite difference scheme on staggered grids. The nonlinear term, viscous term and particle source term were treated explicitly, while the pressure term and equation of continuity were treated implicitly. A second-order Adams–Bashforth method was applied for time marching. The Poisson equation for pressure was solved using Fourier series expansions in the streamwise and spanwise directions together with tridiagonal matrix inversion.

2.2. *Particle motion*

The algorithm for calculation of inter-particle collision is a key issue in this work, because it greatly affects the computation time. We followed the technique of uncoupling developed by Bird (1976), in which the calculation of particle motion is split up into two stages. In the first stage, all particles are moved based on the equation of motion without inter-particle interactions. In the second stage, the occurrence of particle–wall and particle–particle collisions during the first stage is examined for all particles, and, if a particle is found to collide with another particle, the velocities of the collision pair are replaced by post-collision ones without changing their position. This technique of uncoupling requires that the computational time step must be much smaller than the mean free time, which is discussed later.

In our simulations all individual real particles are tracked, not just a number of representative particles.

2.2.1. *Particle motion without collision*

The motion of a small rigid sphere in a turbulent flow field is described by a complicated integro-differential equation (Maxey & Riley 1983). However, if the density of the particle is substantially larger than the density of the carrier fluid, the equation of particle motion can be simplified. The equation of translational motion used in these simulations is

$$\left.\begin{aligned}
m_p \frac{\mathrm{d}\boldsymbol{u}_p}{\mathrm{d}t} &= \boldsymbol{f}_f + m_p \boldsymbol{g}, \\
\boldsymbol{f}_f &= \tfrac{1}{2}\rho|\boldsymbol{u}_R|A\left(C_D\boldsymbol{u}_R + C_{LR}\boldsymbol{u}_R \times \frac{\boldsymbol{\omega}_R}{|\boldsymbol{\omega}_R|}\right) + \boldsymbol{f}_{LG},
\end{aligned}\right\} \tag{2.7}$$

where m_p is particle mass, $\boldsymbol{u}_p$ particle velocity, C_D drag coefficient, ρ gas density, A projected area of particle, C_{LR} lift coefficient due to particle rotation, $\boldsymbol{\omega}_R$ particle rotational velocity relative to gas vorticity, $\boldsymbol{u}_R$ gas velocity relative to the particle and $\boldsymbol{g}$ is acceleration due to gravity. The first term in the right-hand side of equation (2.7) expresses the drag force, the second term the lift force due to rotational motion, $\boldsymbol{f}_{LG}$ the lift force due to velocity gradient and the last term is the gravitational force. The empirical relation for C_D by Schiller & Nauman (1933) was employed,

$$C_D = \frac{24}{Re_p}(1 + 0.15Re_p^{0.687}), \tag{2.8}$$

where Re_p is the particle Reynolds number, $Re_p = d_p|\boldsymbol{u}_R|/v$ (d_p is particle diameter, v is kinematic viscosity of gas). The lift coefficient C_{LR} was obtained from the experimental

Re_R	0–1	1–10	10–20	20–50	50+
C_1	0	0	5.32	6.44	6.45
C_2	50.27	50.27	37.2	32.2	32.1
C_3	0	0.0418	5.32	6.44	6.45

TABLE 1. Torque coefficients of equation (2.12) for the range of rotational Reynolds number.

data by Maccoll (1928) and Davies (1949) according to

$$C_{LR} = \min\left[0.5, 0.25\frac{d_p|\boldsymbol{\omega}_R|}{|\boldsymbol{u}_R|}\right]. \tag{2.9}$$

On average the Magnus lift force is at least one order of magnitude lower than the other forces (Elghobashi & Truesdell 1992), but in the near-wall region particle rotational velocity may reach high values due to the steep velocity gradient and the collision with the wall may increase the rotational velocity, so the effect of particle rotation was taken into account.

In channel flow, the wall-normal component of the lift force $\boldsymbol{f}_{LG}$ should be considered due to the steep velocity gradient. We employed Saffman's expression (Saffman 1965) for $\boldsymbol{f}_{LG}$,

$$f_{LG2} = 1.62 d_p^2 \rho \left(v\left|\frac{\partial u_{R1}}{\partial x_2}\right|\right)^{1/2} \frac{\partial u_{R1}/\partial x_2}{|\partial u_{R1}/\partial x_2|} u_{R1}, \tag{2.10}$$

where x_1, x_2, and x_3 are the streamwise, wall-normal, and spanwise coordinates as shown in figure 1. In our simulation, particle Reynolds number was larger than 1 and in such conditions Wang et al. (1997) showed theoretically that Saffman's expression overestimates the lift force. But experiments by Hall (1988) showed that the measured lift force is larger than the estimation by Saffman's expression. And the results of numerical simulation of vertical pipe flow by Tanaka & Tsuji (1991), in which lift force and inter-particle collision are dominant and Saffman's expression was used for lift force, are in good agreement with experimental measurements. So we used Saffman's expression following Tanaka & Tsuji.

The equation of rotational motion of a particle is

$$I\frac{\mathrm{d}\boldsymbol{\omega}_p}{\mathrm{d}t} = -C_T\frac{\rho}{2}\left(\frac{d_p}{2}\right)^5 |\boldsymbol{\omega}_R|\boldsymbol{\omega}_R, \tag{2.11}$$

where $\boldsymbol{\omega}_p$ is particle rotational velocity and I is the particle's moment of inertia. The right-hand side of equation (2.11) is the viscous torque against particle rotation, which was theoretically obtained by Dennis, Singh & Ingham (1980) and Takagi (1977). C_T is a non-dimensional coefficient which is a function of the Reynolds number for the rotational motion $Re_R = d_p^2|\boldsymbol{\omega}_R|/4v$, given by

$$C_T = \frac{C_1}{(Re_R)^{1/2}} + \frac{C_2}{Re_R} + C_3 Re_R, \tag{2.12}$$

where coefficients C_1, C_2, C_3 are presented in table 1.

For the gas velocity at a particle position, three-dimensional polynomial interpolation using values at eight grid points surrounding the particle was applied. The accuracy of particle position cannot be maintained due to the technique of uncoupling, so we used a simple interpolation method to minimize the computational effort.
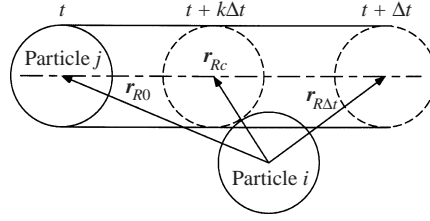
FIGURE 2. Relative motion of colliding particles.

The particle velocity and rotational velocity were integrated by the first-order forward Euler method and the particle position by the second-order Crank–Nicolson scheme.

2.2.2. *Collision*

Only binary collision was taken into account because particle concentration was assumed to be sufficiently low that binary collisions are overwhelmingly dominant. In this work, particle number density is so low that a statistical method for treating the occurrence of collisions (Yonemura *et al.* 1993 and Sommerfeld 1995) cannot be used, so we used a deterministic method (Tanaka & Tsuji 1991).

An outline of the procedure is as follows. Let us consider that a particle i collides with particle j during one time step Δt_c. The particles are assumed to have constant velocities during this time step. Figure 2 shows the relative motion of particles i and j, where $r_R(\equiv r_j - r_i)$, is the relative position vector. The relative distance between the two particles is given by $|r_{R0} + k(r_{R\Delta t} - r_{R0})|$, where k represents a non-dimensional time normalized by Δt_c. The condition for a collision during this time step is that the following equation for k has two real roots k_1 and k_2 ($k_1 < k_2, 0 \leqslant k_1 < 1$):

$$|r_{R0} + k(r_{\Delta t} - r_{R0})|^2 = d_p^2. \tag{2.13}$$

The relative position vector of the contact point to particle i is given by

$$r_{Rc} = r_{R0} + k_1(r_{\Delta t} - r_{R0}). \tag{2.14}$$

Inter-particle collisions are located by evaluating the roots of equation (2.13) for all neighbouring particles.

Post-collisional velocities $\tilde{u}_p$ and angular velocities $\tilde{\omega}_p$ of particles i and j are given by the equations of impulsive motion:

$$\tilde{u}_{pi} = u_{pi} + \frac{J}{m_p}, \tag{2.15}$$

$$\tilde{u}_{pj} = u_{pj} - \frac{J}{m_p}, \tag{2.16}$$

$$\tilde{\omega}_{pi} = \omega_{pi} + \frac{d_p}{2I} n \times J, \tag{2.17}$$

$$\tilde{\omega}_{pj} = \omega_{pj} + \frac{d_p}{2I} n \times J. \tag{2.18}$$

J is the impulsive force exerted on particle i and n is the normal unit vector directed from the centre of particle i to the contact point given by $n = r_{Rc}/|r_{Rc}|$. Assuming spherical particles, a constant coefficient of restitution e for all collisions and negligible particle deformation, J can be calculated from (Tanaka & Tsuji 1991)

$$J = J_n n + J_t t, \tag{2.19}$$

$$J_n = (1+e)M\boldsymbol{c} \cdot \boldsymbol{n}, \tag{2.20}$$

$$J_t = \min\left[-\mu_f J_n, \tfrac{2}{7}M|\boldsymbol{c}_{fc}|\right]. \tag{2.21}$$

In the above equations, $\boldsymbol{t}$ is the tangential unit vector in the direction of the slip velocity of the particle j to i, e is the coefficient of restitution, μ_f is the coefficient of friction and $M = m_p/2$ for collision with another particle and $M = m_p$ for collision with the wall. $\boldsymbol{c}$ is the relative velocity of the centres of mass,

$$\boldsymbol{c} = \boldsymbol{u}_{pj} - \boldsymbol{u}_{pi},$$

and $\boldsymbol{c}_{fc}$ is the slip velocity between particle surfaces,

$$\boldsymbol{c}_{fc} = \boldsymbol{c} - (\boldsymbol{c} \cdot \boldsymbol{n})\boldsymbol{n} - \tfrac{1}{2}d_p\boldsymbol{\omega}_{pi} \times \boldsymbol{n} - \tfrac{1}{2}d_p\boldsymbol{\omega}_{pj} \times \boldsymbol{n}.$$

For inter-particle collision, the velocities and rotational velocities are updated according to equation (2.15)–(2.18). For particle–wall collision, the time interval Δt is subdivided into Δt_w and $\Delta t - \Delta t_w$, where Δt_w is the time before the collision. Each particle is moved in the first interval (Δt_w) using the pre-collision quantities, and moved in $\Delta t - \Delta t_w$ according to the post-collision values.

3. Simulation conditions
3.1. *Effect of spatial resolution of LES on particle motion*
When the particle Stokes number is large, the effect of SGS eddies on particle motion is negligible. However, particles that have a small Stokes number can be affected by the SGS eddies. In this section, we examine the effect of small-scale motion of the fluid on the particle motion to confirm that the effect of SGS eddies on the particle motion is negligible. As a result, the spatial resolution of LES required to resolve the particle motion is determined.

Wang & Squires (1996) estimated the effect of SGS fluctuating velocity on the motion of light particles using the transport equation of SGS kinetic energy. However, models are required in the equation of SGS kinetic energy and in transforming SGS energy to SGS fluctuation velocity. On the other hand, we directly examined the effect of small eddies on the motion of particles by simultaneously calculating their trajectories in a highly resolved flow field (which is called 'raw flow field' hereinafter) and in filtered flow fields obtained by a sharp cutoff filter at over twenty cutoff wavenumbers. The raw flow field was calculated by LES with high-resolution grids. The effect of small-scale eddies was studied by comparing particle trajectories in the raw flow field with those in filtered flow fields.

3.1.1. *Procedure for validation of spatial resolution*
Initially, 4800 particles were distributed uniformly in the computational domain. A fully developed state was used as the initial condition of the gas flow field. The initial velocity and rotational velocity of particles were given the same values as those of the gas at each particle position. The gas flow in the raw flow field was solved with the high-resolution grid. The number of grid points was 128 in each direction. The grid spacing in the streamwise and spanwise directions was 22.5 and 7.5 in wall units, while that in the wall-normal direction was between 1.96 (nearest the wall) and 19.6 (at the channel centre). The time increment Δt used in the simulations was 0.13 in wall units (8.2×10^{-6} s). For the calculations described in this section, the fluid flow field was calculated by one-way coupling, i.e. f_{pi} in equation (2.6) was set to zero because only the effect of turbulent motion of gas on particle motion was examined.

Density ρ_p [kg m^{-3}]	700	700	2500	2500	2500	8800
Diameter d_p [μm]	7	28	25	50	90	70
Stokes relaxation time τ_p [ms]	0.11	1.7	4.8	19	63	133
$St^+ \equiv \tau_p/(v/u_\tau^2)$	2	27	76	301	998	2110

TABLE 2. Properties of particles for validation of spatial resolution.

At each time step the highly resolved flow field was filtered by cutting off high wavenumber components in the wavenumber space. The motion of particles with the same initial conditions was calculated simultaneously in the raw flow field and filtered flow fields. Since the grid resolution was different for each direction, one-dimensional filtering was applied in the streamwise and spanwise directions respectively. FFT was not possible in the wall-normal direction due to the non-uniform grid, so we did not apply filtering in that direction.

The particle position in a filtered flow field deviates from that in the raw flow field as time increases. This instantaneous deviation D in particle position was used to measure the effect of filtering on the particle motion. In channel flows, statistical properties are functions of the distance y from the wall, so averages of D are taken at each y-position. To evaluate the effect of fluid motion on particle motion, we could examine the variance of the particle velocities. But we used the mean of deviation of the particle path because it is difficult to imagine the effect of the difference of variance on the formation of the particle cloud.

We used six kinds of particles, whose properties (table 2) are the same as those in the experiments by Kulick *et al.* (1994) and Fessler *et al.* (1994), the DNS by Rouson & Eaton (1994) and the LES by Wang & Squires (1996). The particle relaxation time τ_p, representing the time required to respond to the surrounding fluid, was estimated by the following expression for Stokes flow:

$$\tau_p = \frac{\rho_p d_p^2}{18\rho v}. \tag{3.1}$$

Although not all particles studied here obey the assumption of Stokes flow, we used the relaxation time of (3.1) for convenience. St^+ in table 2 is Stokes number based on particle relaxation time and the flow time scale in wall units,

$$St^+ = \frac{\tau_p}{v/u_\tau^2}. \tag{3.2}$$

Normalization of grid resolution for channel flow simulations is often based on wall variables (i.e. friction velocity and kinematic viscosity), so that all results in this section are non-dimensionalized by wall variables.

3.1.2. *The effect of filtering on the gas phase*

To see the effect of filtering on the gas flow field the distributions of enstrophy $(1/2)\omega_i'\omega_i'$ in the planes $y^+ = 644$ and $y^+ = 110$ are shown in figure 3. The size of the area shown is 2880 in the streamwise direction and 960 in the spanwise direction in wall units. It can be seen that the small-scale fluctuation intensity, and consequently the effect of filtering, is higher in the near-wall region than in the channel centre.
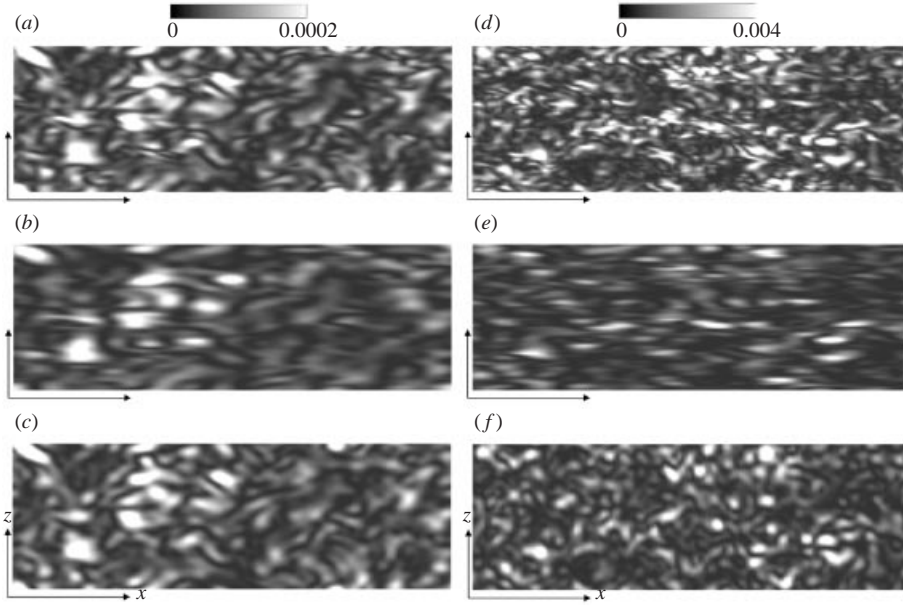
FIGURE 3. Filtered fields, $(1/2)\omega_k^{+\prime}\omega_k^{+\prime}$ contours at the channel centreplane, (a, b, c) at the channel centre ($y^+ = 644$) and (d, e, f) near the wall ($y^+ = 110$). λ^+ is the cutoff wavelength normalized by wall variables. The size of the area shown is 2880 in the streamwise direction and 960 in the spanwise direction in wall units. (a, d) Highest resolution, (b, e) filtered in the x-direction at $\lambda_x^+ = 360$, (c, f) filtered in the z-direction at $\lambda_z^+ = 120$.

3.1.3. *The effect of filtering on particle motion*

Figures 4 and 5 show the deviation of particle trajectories in the filtered fields from those in the raw flow field, for particles initially at the channel centre (figure 4) and near the wall ($y^+ = 110$; figure 5). The abscissa is wavelength of cutoff filter scale λ_i^+ ($i = x, z$) and the ordinate is the deviation normalized by the diffusive length scale $u_{irms}' T$, in which u_{irms}' is the gas turbulence intensity and T is the period of simulation, which was set to $100\nu/u_\tau^2$ s. Figures 4 and 5 show that the particle motion is not affected by λ_i^+ in a significant region of small λ_i^+. This result means that the spatial resolution of raw flow field is sufficient to resolve particle motion. When λ_i^+ exceeds a certain value the deviation increases with λ_i^+. From these figures, it is apparent that the lower the particle Stokes number, the larger the effect of small-scale eddies on the particle motion. In some plots, the magnitude of D is not correlated well with St^+ at large wavelength, perhaps because the time length T in which D is examined is small compared with the time scale of the turbulence event. Comparing figures 4 and 5, the effect of filtering is found to be more significant in the near-wall region than in the channel centre.

Defining a critical cutoff wavelength λ_{icut}^+, as the wavelength which gives 0.3% deviation, figure 6 shows λ_{icut}^+ versus Stokes number for each initial y-position. Confirming the general tendency of figures 4 and 5, λ_{icut}^+ clearly increases with St^+. The rate of increase is very marked in the range $St^+ > 1000$, and moderate in the range $St^+ < 1000$. This figure shows that the spatial resolution in the z-direction should be higher than in the x-direction.
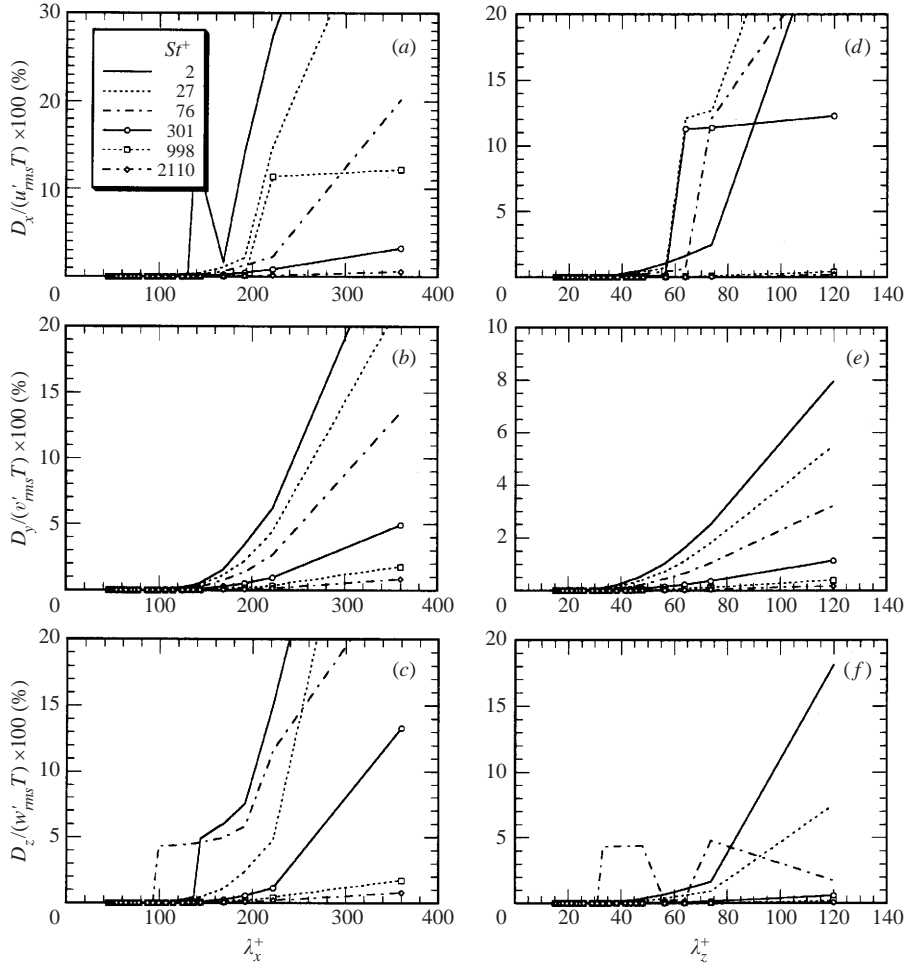
FIGURE 4. Deviation by the x-filter (a, b, c) and by the z-filter (d, e, f), at the channel centre $(y_0^+ = 644)$ normalized by the diffusive length scale. (a, d) x-component, (b, e) y-component, and (c, f) z-component.

3.1.4. *Analysis of the relation between St^+ and λ_{icut}^+*

Here we make a simple analysis of the relation between St^+ and λ_{icut}^+ based on time scales to interpret physically the trend of the calculated results. The time during which a particle's motion is affected by an eddy is characterized by the eddy lifetime τ_e or the eddy crossing time τ_c, whichever is shorter. When the particle response time τ_p is smaller than both of these time scales, the particle motion is affected by the eddy. In the critical case,

$$\frac{\tau_p}{\tau_c} \sim 1 \quad (\tau_c < \tau_e), \tag{3.3a}$$

$$\frac{\tau_p}{\tau_e} \sim 1 \quad (\tau_c > \tau_e), \tag{3.3b}$$

where $\tau_p = \rho_p d_p / (18\mu)$, $\tau_c = l_e / \overline{u_p}$ (l_e being the length scale of the smallest eddy that can affect the particle motion, and $\overline{u_p}$ mean particle velocity relative to the eddy). We
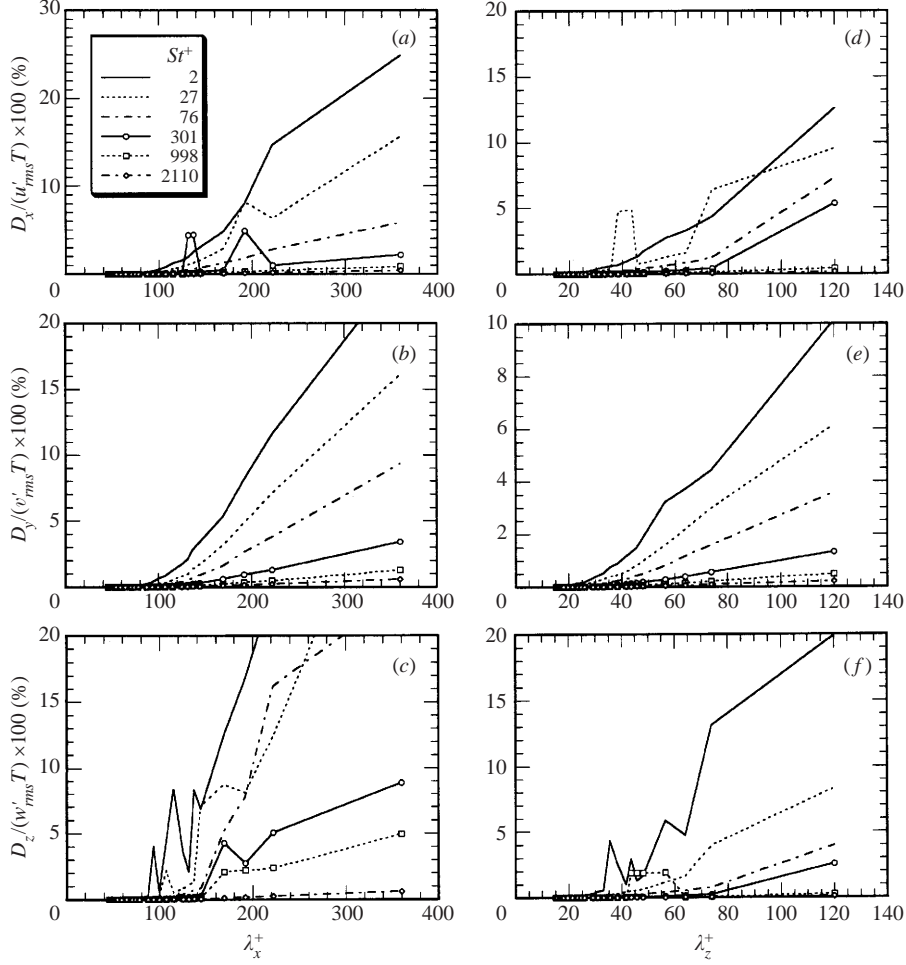
FIGURE 5. Deviation by the x-filter (a, b, c) and by the z-filter (d, e, f), near the wall $(y_0^+ = 110)$ normalized by the diffusive length scale. (a, d) x-component, (b, e) y-component, (c, f) z-component.

assumed that the kinetic energy of the eddy is completely dissipated by viscosity,

$$\tfrac{1}{2}\rho l_e^3 v_e^2 \sim l_e^2 \rho v \frac{v_e}{l_e} v_e \tau_e,$$

where l_e and v_e are the length and velocity scales of the eddy. With this assumption, the eddy lifetime τ_e is estimated as $\tau_e \sim l_e^2/v$. Furthermore, we assume that the critical cutoff wavelength is given by $\lambda \sim l_e$, and $\overline{u_p} \sim \tau_p g$ ($\tau_p g$ corresponds to the terminal velocity). Then, the critical cutoff wavelength λ_{icut} is expressed by

$$\lambda_{icut} \sim g\tau_p^2 \ (\tau_c < \tau_e), \tag{3.4a}$$

$$\lambda_{icut} \sim (v\tau_p)^{1/2} \ (\tau_e < \tau_c), \tag{3.4b}$$

or as a function of St^+ in wall units,

$$\lambda_{icut}^+ \sim \frac{gv}{u_\tau^3}(St^+)^2 \ (\tau_c < \tau_e), \tag{3.5a}$$

$$\lambda_{icut}^+ \sim (St^+)^{1/2} \ (\tau_e < \tau_c). \tag{3.5b}$$
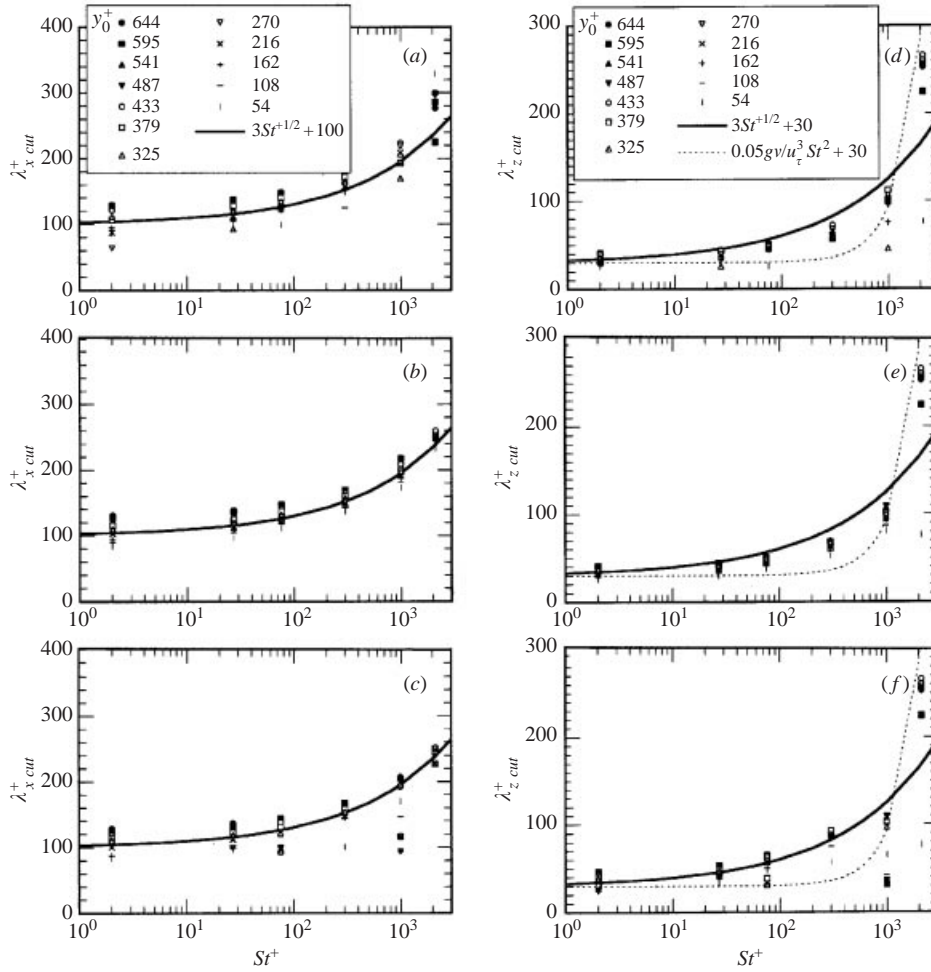
FIGURE 6. Cutoff wavelength at 0.3% deviation by the x-filter (a, b, c) and by the z-filter (d, e, f). (a, d) x-component, (b, e) y-component, (c, f) z-component.

In figure 6, curves of equations (3.5) are also shown, multiplied by appropriate coefficients and offset by a constant so as to fit the numerical results. Equations (3.5) express qualitative trends well and show that the change at $St^+ = 1000$ is due to the change of the time scale governing the phenomena. From the results in figure 6, for particles of $St^+ > 20$ a grid spacing of $\Delta x^+ = 45$, $\Delta z^+ = 15$ (corresponding to wavelength of $\lambda_x^+ = 90$ and $\lambda_z^+ = 30$) is large enough to calculate the particle dispersion correctly within an error of 0.3% of the characteristic length scale when $t^+ = 100$.

3.2. *Conditions for the two-phase flow simulation*

Table 3 shows the properties of the particles used in our simulations. Stokes number $St \equiv \tau_p/\tau_f$ in table 3 is based on τ_p and the time scale of the large eddy estimated from channel half-width and channel centreline velocity $\tau_f = \delta/U_{cl}$. Stokes number based on Kolmogorov time scale $\tau_k = (\nu/\epsilon)^{1/2}$ is often used. In LES, however, the dissipation rate cannot be estimated precisely and τ_f and τ_k are almost the same for the conditions of this study (Fessler *et al.* 1994), so the results of this study use the Stokes number based on the time scale of the large eddies.

Material	Copper	Copper	Glass	Lycopodium
Density ρ_p [kg m^{-3}]	8800	8800	2500	700
Diameter d_p [μm]	70	70	50	28
Stokes relaxation time τ_p [ms]	130	130	18	1.7
Stokes number $St \equiv \tau_p/(\delta/U_{cl})$	70	70	10	0.89
Loading ratio ϕ	0.2	1	0.2	0.01
Solid volume fraction [$\times 10^{-4}$]	0.27	1.4	0.96	0.17
Number of particles	15 889	79 445	154 214	156 159

TABLE 3. Properties of particles used in the simulations.
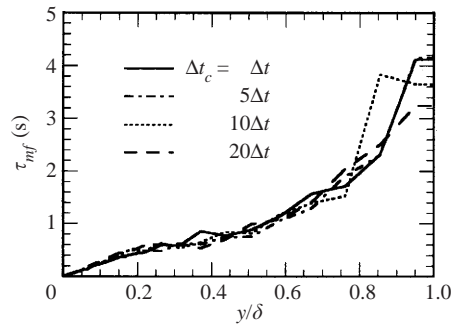
FIGURE 7. Mean free time of a lycopodium particle calculated for various time steps.

The simulations were performed with $64 \times 48 \times 64$ grid points in the x-, y- and z-directions. The grid spacing given in wall units was $\Delta x^+ = 45$, $\Delta z^+ = 15$ and $\Delta y_{min}^+ = 2.8$ to the wall and $\Delta y_{max}^+ = 63.3$ at the channel centre. This spatial resolution was found to be high enough in the x- and z-directions to calculate the particle motion accurately as mentioned above. The grid spacing in the y-direction may be thought to be too large in the channel-centre region. In our simulations all individual real particles are tracked, not a number of representative particles. The results of the instantaneous structure of particle distribution and its statistics are good agreement with experimental results as shown later, so the grid spacing in the y-direction is adequate.

The time step for calculation of fluid motion and for particle motion free from collisions was $\Delta t = 2 \times 10^{-4}\delta/u_\tau = 8.205 \times 10^{-6}$ s. This time step was confirmed by the calculated results to be small enough that particles and fluid elements cannot pass through a computational cell during one time step.

The calculation of inter-particle collisions takes much computational time so we tried to reduce the computation by not calculating inter-particle collisions at every time step. If the time step is much smaller than the mean free time, the technique of uncoupling can be applied and inter-particle collisions need not be calculated at each time step. Figure 7 shows the mean free times of collision for a lycopodium particle, whose condition is most severe, calculated by short period simulations. It was found that $5\Delta t(= 4.1 \times 10^{-5}$ s$)$ is smaller than the minimum mean free time of 6.5×10^{-4} s and results were the same for every step calculation. So a collision calculation was carried out once per 5 steps, which corresponds to setting the time step for collision calculation to $\Delta t_c = 5\Delta t$. This is much smaller than the particle relaxation time τ_p, so that inter-particle collisions are calculated assuming particle motion is linear during Δt_c.
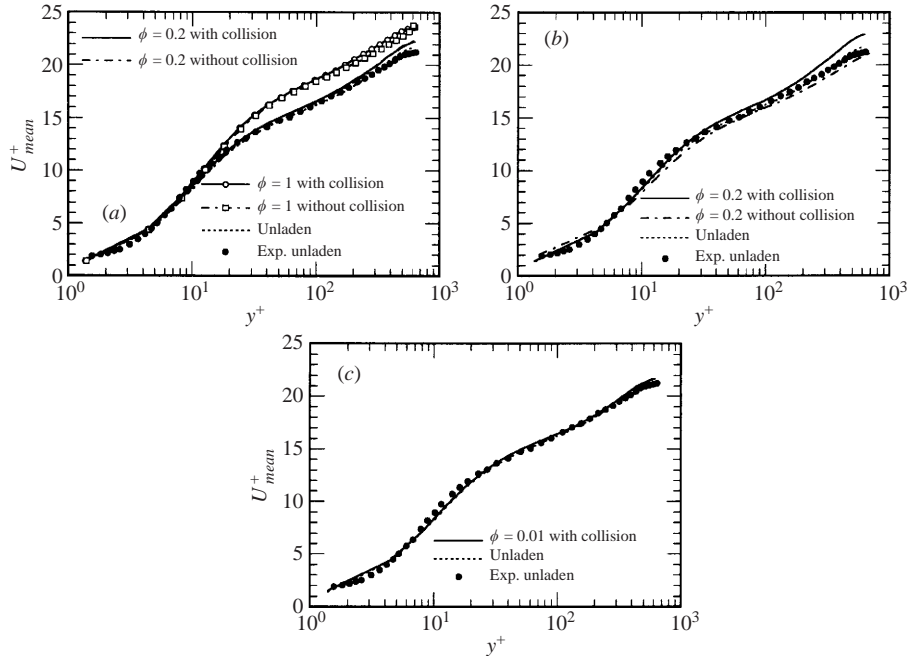
FIGURE 8. Gas-phase mean streamwise velocity profiles (experimental data by Kulick *et al.* 1994): (*a*) copper, (*b*) glass, (*c*) lycopodium.

In this study we chose the coefficient of restitution as 0.95 and the coefficient of friction as 0.3, which are roughly appropriate for the materials in our simulations.

At the beginning of the two-phase flow simulations for each particle size and loading, a fully developed flow field calculated by a single-phase calculation was specified and particles were distributed uniformly in the computational domain by random numbers, with the velocities of the particles being the fluid velocity at the same position. All statistical and instantaneous analyses were done after confirming that the flow fields had reached fully developed states.

In order to study the effect of inter-particle collision, cases with and without collision were calculated. All the calculations were performed with two-way coupling, except for the case of lycopodium particle without inter-particle collision, which could not be completed because extreme particle concentrations in the near-wall region caused numerical divergence. Accordingly, the results for lycopodium particles without inter-particle collisions were calculated by one-way coupling. Also the results for glass particles with one-way coupling and without inter-particle collision are shown in order to compare with other researchers' results.

All the calculations were run on the NEC SX-3R and SX-4 at Osaka University Computation Center. A lycopodium particle simulation considering inter-particle collisions required the longest computation time, about 20 CPU hours.

4. Results and discussion

4.1. *Mean velocity*

Figure 8 shows mean streamwise gas velocity profiles. The calculated results for single-phase flow agree well with experimental data by Kulick *et al.* (1994). Experimental
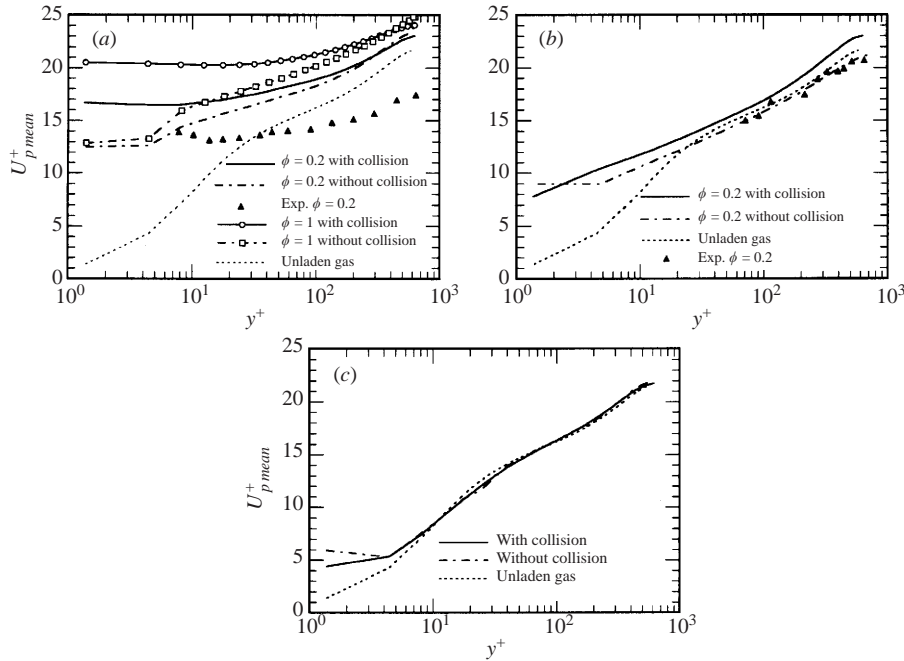
FIGURE 9. Particle mean streamwise velocity profiles (experimental data by Kulick *et al.* 1994): (*a*) copper, (*b*) glass, (*c*) lycopodium.

data of two-phase flow by Kulick *et al.* (not shown in figure) show that mean gas velocity profiles are unchanged by the presence of particles up to a mass loading of $\phi = 0.4$. The present results show that mean gas velocity profiles are unchanged at $\phi = 0.2$. In the case of high mass loading $\phi = 1$, profiles in the logarithmic layer are shifted upward, because particles fall faster than gas, as shown later, so that gas is dragged by particles. Profiles in the near-wall region are unchanged because the wall shear stress of the calculations is set equal to the experiments.

Figure 9 shows mean streamwise particle velocity profiles. Inter-particle collisions strongly affect the profiles: the results of calculations with account taken for inter-particle collision are flatter than those without, and the velocity gradient with collisions considered is close to that of the experimental results. This is related to the fact that with inter-particle collisions the particle fluctuation velocity in the wall-normal direction approaches experimental values as shown in the following section. However, the magnitude of the calculated particle mean velocity is greater than the experimental values. This discrepancy may be because the experimental facility is not long enough to reach a fully developed state or friction between particle and the wall in the experiment is much larger than that in the present simulation. The friction between particle and the wall in the experiments can be large and irregular repulsion can cause large transverse diffusion because the development section of the channel used in the experiment is made of wood. Thus, this discrepancy may be mainly due to this wall roughness effects. In the case of copper particles at $\phi = 1$, taking account of inter-particle collision yields the same trend as for $\phi = 0.2$. The magnitude of velocity in the logarithmic layer for $\phi = 1$ is larger than for $\phi = 0.2$, by an amount equal to the difference in mean gas velocity. Particle mean velocity profiles of glass and lycopodium are the same as mean gas velocity profiles in the logarithmic layer.
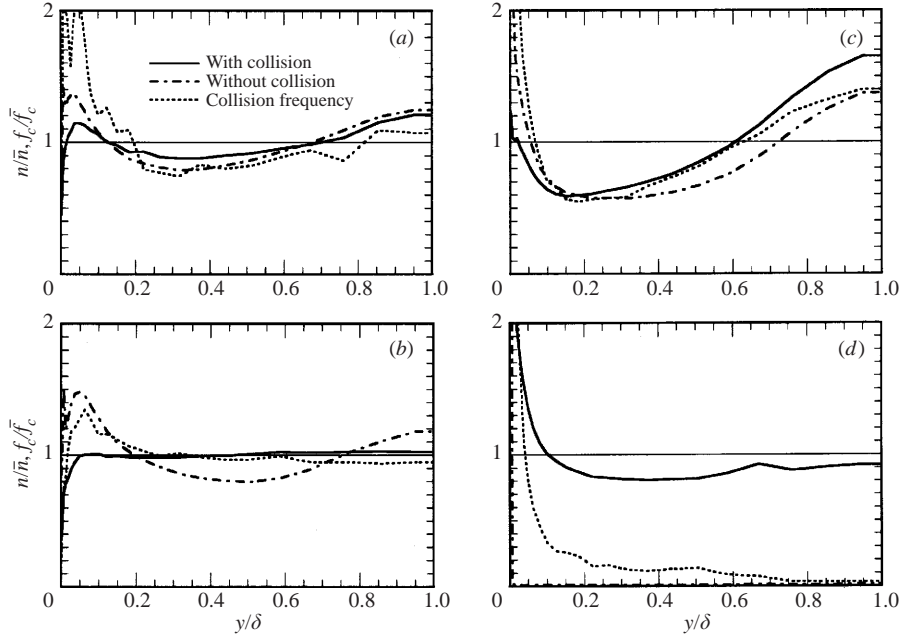
FIGURE 10. Particle number density and collision frequency profile normalized by mean values:
(*a*) copper $\phi = 0.2$, (*b*) copper $\phi = 1$, (*c*) glass, (*d*) lycopodium.

4.2. *Particle concentration*

Figure 10 shows particle number density and collision frequency profiles normalized by mean values. Particle concentrations calculated ignoring inter-particle collisions are high in the near-wall region and in the channel centre region, because particles are transported by the effect of the wall-normal fluctuation velocity of the fluid, which is small in both regions. In the near-wall region, because the slip velocity and gradient of gas velocity are high, particles are trapped by the effect of the force due to velocity gradient. Inter-particle collisions make profiles of particle concentration flatter, remarkably so in the case of high loading. Collision frequency profiles show that particles collide most frequently in the region where particles would be highly concentrated without collisions, i.e. near the wall. Low-inertia particles concentrate in the near-wall region, and in particular in the case of lycopodium almost all particles are in the near-wall region when collisions are ignored. In the case of lycopodium particles with inter-particle collision, the number density is nearly constant about the mean value except in the near-wall region, while collision frequency is sharply peaked near the wall.

4.3. *Particle fluctuation velocity*

Figure 11 shows profiles of r.m.s. streamwise particle fluctuating velocity. To compare numerical and experimental results, we focus on copper at $\phi = 0.2$ (figure 11*a*) and glass (figure 11*c*). In the region of y^+ where experimental data exist, the effect of inter-particle collision can be neglected, as judged by comparison of the computational profiles. In the case of copper, calculated results agree well with experimental results except in the channel centre. Calculated results for glass particles are slightly above the experimental values; however they represent the trend of the experimental results quite well. In these dilute conditions, streamwise particle fluctuation intensity is
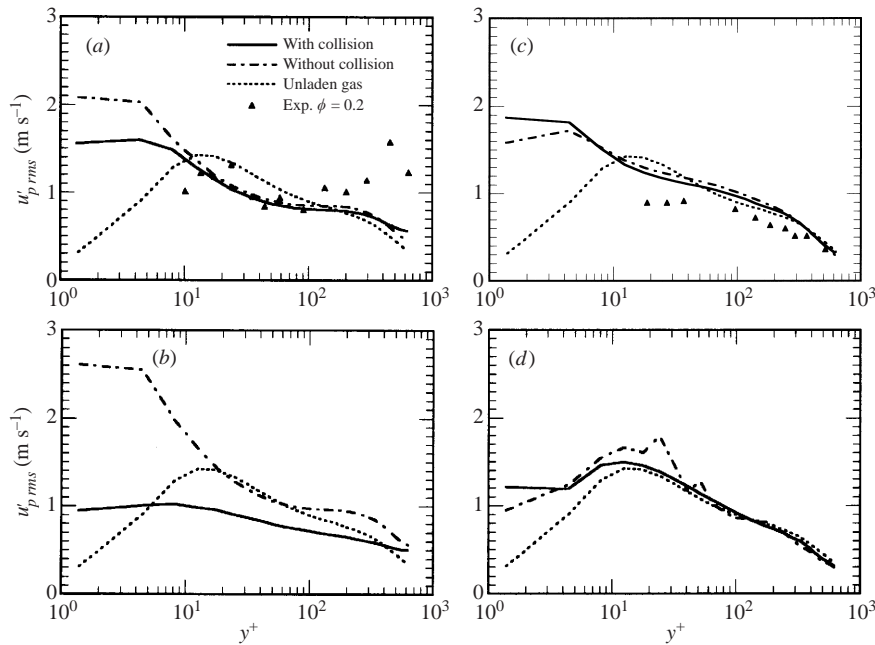
FIGURE 11. Fluctuation intensity profiles of streamwise particle velocity (experimental data by Kulick *et al.* 1994): (*a*) copper $\phi = 0.2$, (*b*) copper $\phi = 1$, (*c*) glass, (*d*) lycopodium.

the same as gas turbulence intensity except in the near-wall region, where in both cases, fluctuation intensities are high. That is because streamwise velocities which are involved when particles collide with the wall are decreased by friction, and because the gas velocity has a steep gradient. It should be noted that inter-particle collisions reduce the streamwise fluctuation intensity, because streamwise velocity is converted to normal velocity by inter-particle collisions, as discussed later. At $\phi = 0.2$, the effect of inter-particle collisions on streamwise fluctuation intensity is small, but in the case of high loading the effect becomes very significant, as seen in figure 11(*b*) where inter-particle collision reduces fluctuation velocity substantially. In the case of lycopodium particles (figure 11*d*), particle fluctuation velocity is almost the same as that of the gas except in the near-wall region.

Figure 12 shows wall-normal particle fluctuation intensity profiles. In the case of copper at $\phi = 0.2$, the calculated results both with and without collision are distributed uniformly, like the experimental results, but ignoring inter-particle collisions reduces the intensity to a level much lower than the experimental results. The same effect appears even more strongly in the case of copper $\phi = 1$ (figure 12*b*) and glass (figure 12*c*). In the case of lycopodium (figure 12*d*), there is no obvious effect of inter-particle collision, because particle inertia is small. Calculated profiles of spanwise particle fluctuation intensity not presented in this paper show the same trend as wall-normal components, i.e. the profiles are flat and the magnitude is substantially increased by inter-particle collisions.

Summarizing the results of figures 11 and 12, and those for the spanwise particle fluctuations (not shown), inter-particle collision reduces streamwise fluctuation velocity and increases normal fluctuations by a corresponding amount in the region $10 < y^+ < 300$, i.e. inter-particle collisions convert streamwise fluctuation energy to fluctuation energy normal to the mean flow. In the near-wall region ($y^+ < 10$), the
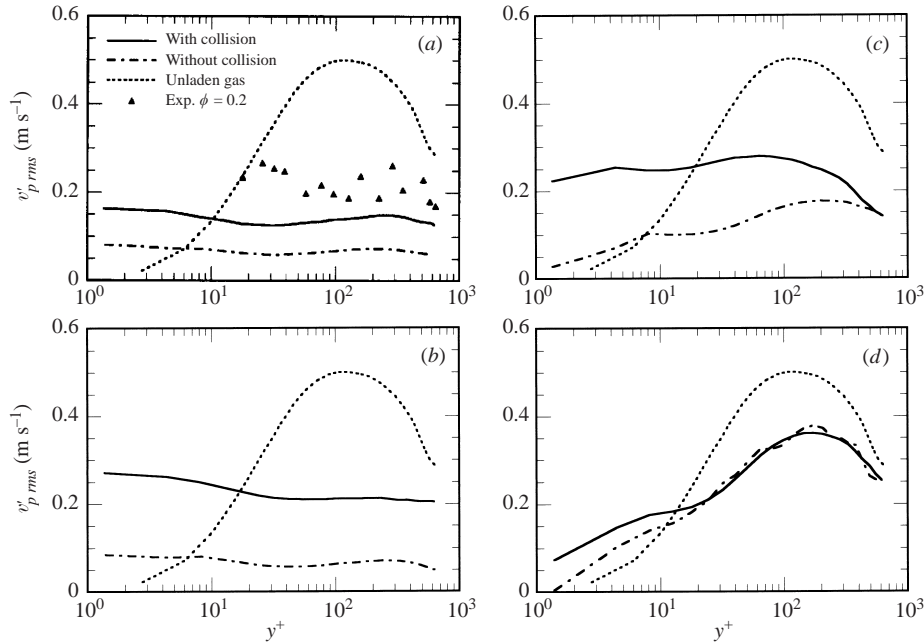
FIGURE 12. Fluctuation intensity profiles of wall-normal particle velocity (experimental data by Kulick *et al.* 1994): (*a*) copper $\phi = 0.2$, (*b*) copper $\phi = 1$, (*c*) glass, (*d*) lycopodium.

amount of reduction and increase were not the same because of the effect of the wall. In the region of large velocity gradient ($y^+ < 300$), streamwise fluctuation is produced by particle mixing in the wall-normal direction, while in the channel-centre region ($y^+ > 300$), the velocity gradient is small, so the trend there differs.

Thus, there is a very large effect of inter-particle collisions on particle fluctuating velocity. The increase of wall-normal fluctuation velocity, in particular, flattens profiles of concentration and mean velocity. By taking inter-particle collision into account, calculated results approach experimental ones. It was found that inter-particle collisions cannot be neglected even in these dilute conditions in which particle volume fraction is $O(10^{-4})$.

4.4. *Turbulence intensity of the gas phase*

In this study, the effect of particles on SGS stress is neglected, so the present results do not give information about turbulence modification at small scales. However we can discuss the interaction between large-scale eddies and particles.

Figure 13 shows streamwise turbulence intensity profiles. In the case of copper particles at $\phi = 0.2$ (figure 13*a*), the experimental results show attenuation of turbulence by particles, but the calculated results underestimated this attenuation regardless of whether inter-particle collision was included or not. It is considered that the experimentally observed attenuation of turbulence in this case is due to the effect of the small mean velocity of particles. Large slip velocity in the experiment (see figures 8 and 9), which has opposite sign to that of present simulation, caused large drag force, so that the turbulence of the gas phase was attenuated. In the case of copper particles at high loading, ($\phi = 1$; figure 13*b*), the effect of particles on large-scale eddies in the calculations attenuates turbulence intensity. Without the effect of particles on the SGS model, the trend that the degree of attenuation is increasing with mass loading
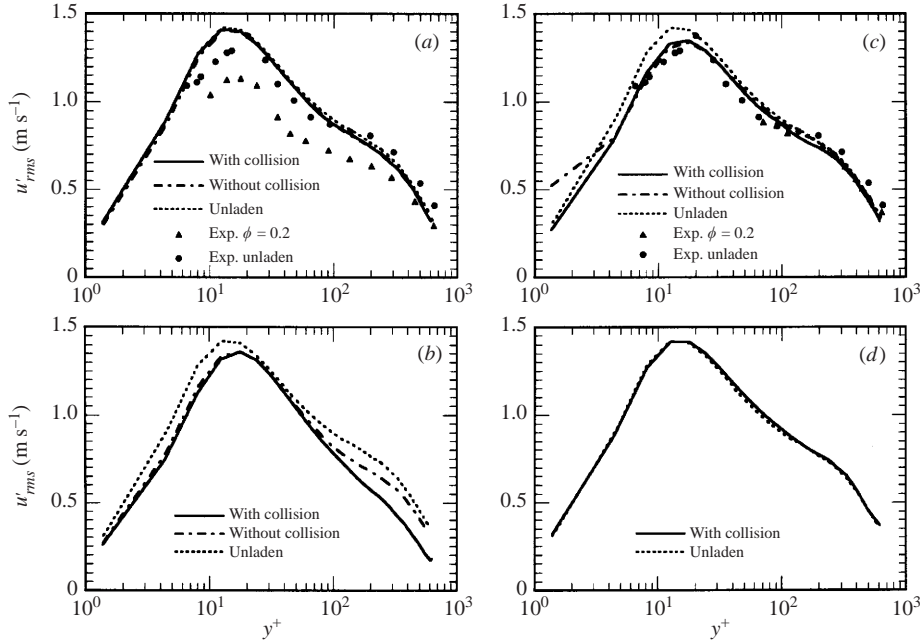
FIGURE 13. Streamwise turbulence intensity profiles (experimental data by Kulick *et al.* 1994): (*a*) copper $\phi = 0.2$, (*b*) copper $\phi = 1$, (*c*) glass, (*d*) lycopodium.

is shown. In the channel-centre region, inter-particle collisions increase attenuation, because energy transferred from turbulence to particles is dissipated by non-elastic collisions and converted to fluctuation velocity in the normal direction as mentioned before.

In the case of glass particles (figure 13*c*), the calculated results show the same order of attenuation as experimental results, unlike the case of copper. This suggests that turbulence attenuation is mainly caused by the effect of particles on large-scale eddies in this case because the SGS model in our calculation does not contain the effect of particles and glass particles form clouds as shown later.

In the case of lycopodium (figure 13*d*), turbulence intensity is not modified by the particles. Profiles of wall-normal and spanwise turbulence intensity for each particle show the same trend as for the streamwise component, so we do not present the data in this paper.

Figure 14 shows the one-dimensional spectrum of streamwise turbulence intensity in the channel centre. For copper particles at $\phi = 0.2$ (*a*), the effect of particles cannot be observed, but at $\phi = 1$ (*b*), it is found that particles reduce the spectral density in the low-wavenumber region and moderate the slope of the spectrum in the high-wavenumber region regardless of inter-particle collision. This trend is accentuated when inter-particle collisions are considered. Thus it appears that inter-particle collisions only modify turbulence under high loading conditions. In the case of glass particles at $\phi = 0.2$ (*c*), attenuation is observed in the range $100 < \kappa_x < 200$, and is independent of whether or not inter-particle collision is considered. Note that a wavenumber of $\kappa_x = 200\,\mathrm{m}^{-1}$ corresponds to 5 mm in length scale. Particle clouds with a scale of several millimetres were observed in the channel-centre region, as presented later, so that gas turbulence would appear to be attenuated by the effect of particle clouds.
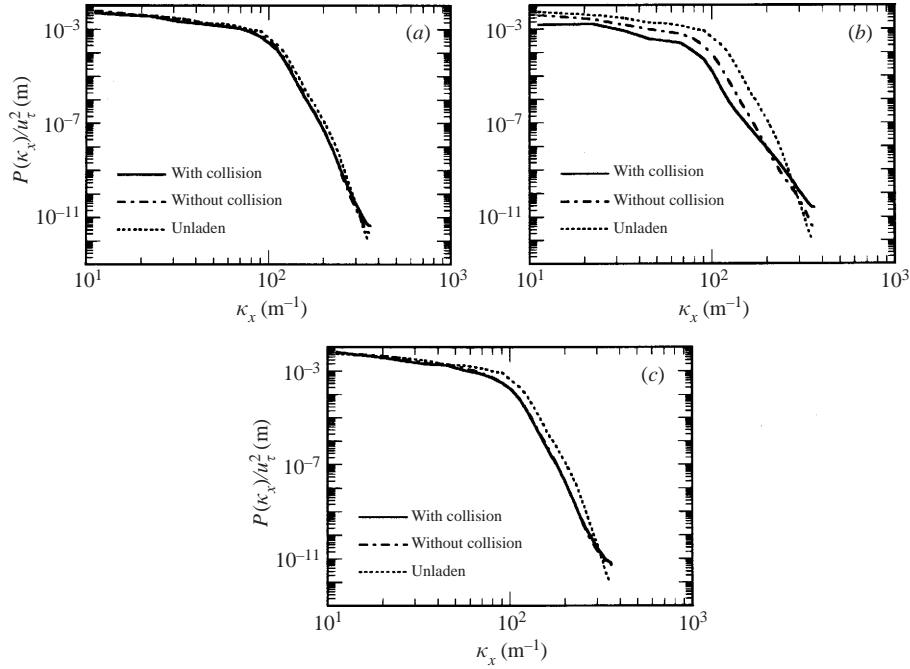
FIGURE 14. Streamwise spatial spectra of streamwise fluctuation velocity at the channel centreline: (*a*) copper $\phi = 0.2$, (*b*) copper $\phi = 1$, (*c*) glass $\phi = 0.2$.
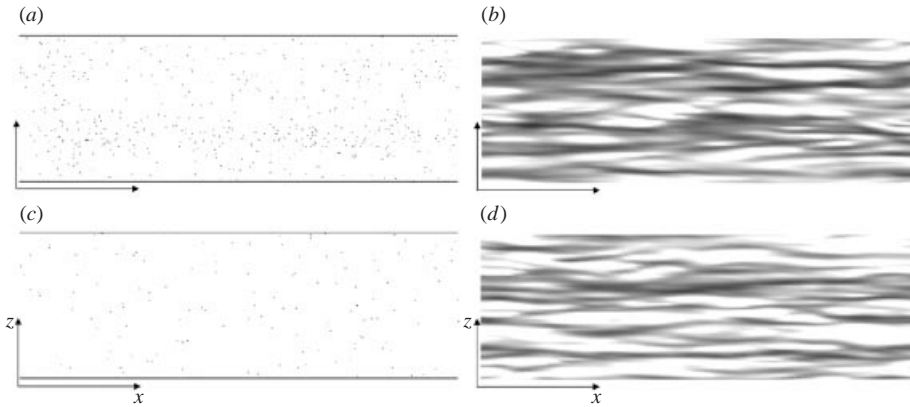

FIGURE 15. Instantaneous distribution of particles and gas streamwise velocity on the wall-parallel plane in the near-wall region, copper $St = 70$, $\phi = 1$ (particle at $y^+ = 0$–4, gas at $y^+ \sim 4$, darker region: low speed, lighter region: high speed). The size of the area shown is 2880 in the streamwise direction and 960 in the spanwise direction in wall units. (*a*) 2-way without collision, particle; (*b*) 2-way without collision, gas velocity; (*c*) 2-way with collision, particle; (*d*) 2-way with collision, gas velocity.

4.5. *Spatial structure in the near-wall region*

In this section, correlations between spatial structure of particle distribution and fluid turbulence in the near-wall region (i.e. viscous sub-layer) are discussed. In our simulations, all individual particles were tracked and fluid velocity at a particle position was interpolated in the calculation of particle motion. Thus we can examine the particle distribution in an arbitrary plane to discuss the spatial structure of particle distribution.
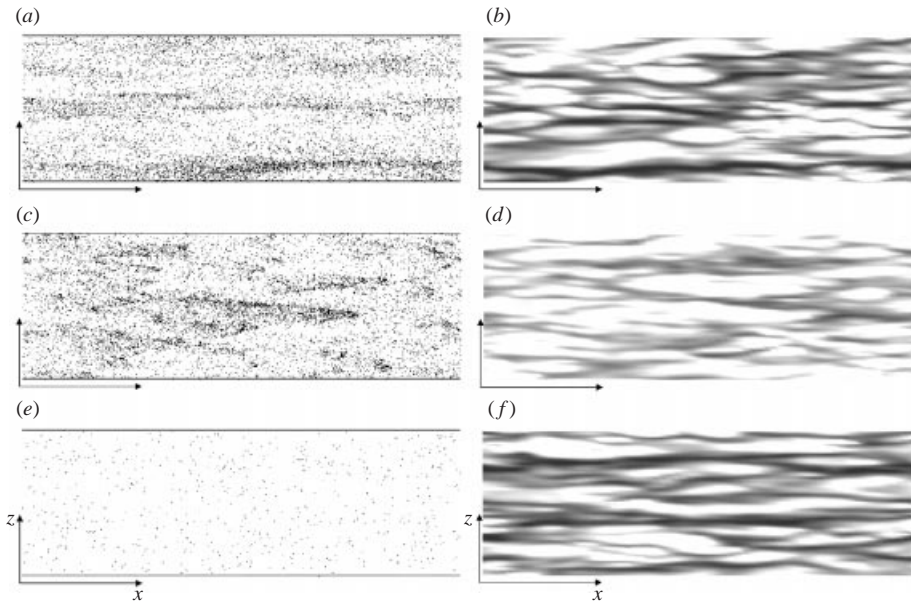
FIGURE 16. As figure 15 but for glass $St = 10$. (*a*) 1-way without collision, particle; (*b*) 1-way without collision, gas velocity; (*c*) 2-way without collision, particle; (*d*) 2-way without collision, gas velocity; (*e*) 2-way with collision, particle; (*f*) 2-way with collision, gas velocity.

Figure 15 shows simultaneous snapshots of copper particle distribution and gas streamwise velocity in the wall-parallel plane at $y^+ \sim 4$. Hereafter, all results for copper particle are for the case $\phi = 1$. Copper particles, which have large inertia, are distributed nearly uniformly and are very dilute in this region regardless of inter-particle collision. Figures 15(*b*) and 15(*d*) show that gas streamwise velocity distributions form a streaky structure. Large-inertia particle are not affected by the small-scale turbulence structure of the gas phase.

Figure 16 shows the instantaneous glass particle distribution and gas streamwise velocity distribution. In the case of one-way coupling without inter-particle collision shown in figure 16(*a*, *b*), streamwise gas velocity distribution has a streaky structure, and particle concentration is high in the low-speed streaks, through the phenomenon referred to as 'preferential concentration'. This result shows the same trend as Rouson & Eaton (1994) and Wang & Squires (1996), which is to be expected because they also neglected inter-particle collisions and applied one-way coupling. Pedinotti *et al.* (1992) suggested that this phenomenon is caused by the effect of quasi-streamwise vortices; particles are transported to the near-wall region by sweeps and accumulate in ejection regions.

By contrast, in the case of two-way coupling without inter-particle collision (figure 16*c*, *d*), gas velocity is high in regions of high particle concentration, because the gravitational force on particles is transmitted to the fluid in dense regions. In the present calculation gas flows downward (i.e. gravity direction), so that gas is entrained by particles more strongly in regions of high particle concentration than in dilute regions. Thus when preferential concentration occurs, one-way and two-way coupling calculations show completely different results. In the case of two-way coupling with inter-particle collisions (figure 16*e*, *f*), particle concentration in the near-wall region is low because the inter-particle collision disperses particles in the wall-normal direction and no streaky particle distribution is observed.
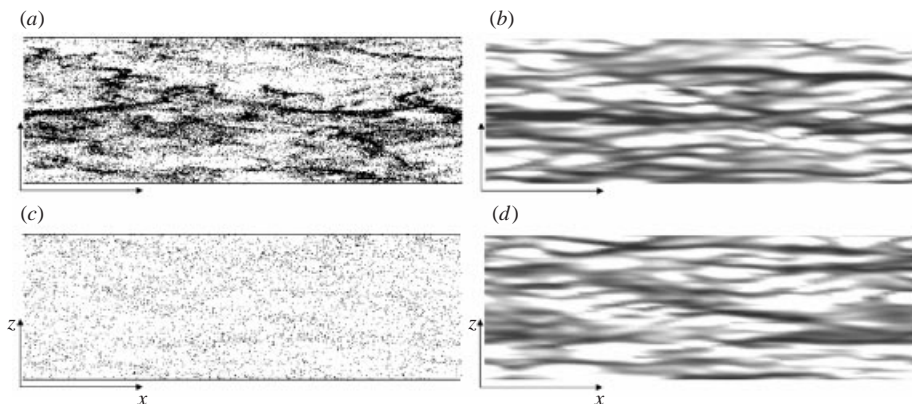
FIGURE 17. As figure 15 but for lycopodium $St = 0.89$. (*a*) 1-way without collision, particle; (*b*) 1-way without collision, gas velocity; (*c*) 2-way with collision, particle; (*d*) 2-way with collision, gas velocity.

Figure 17 shows corresponding snapshots for lycopodium particles. One-way coupling without inter-particle collision (figure 17*a*, *b*), yields high particle concentration in the low-speed regions as with glass particles, but particles are more clearly concentrated into 'clouds', and the size of clouds is smaller than for glass particles. In the case of two-way coupling with inter-particle collision (figure 17*c*, *d*), particles are dispersed by inter-particle collisions so that particle concentration is low in the near-wall region. No obvious correlation between particle concentration and turbulence structure was found.

Following the comparison of instantaneous structures, let us now consider the statistical correlation between particle concentration and gas velocity. Following Pedinotti *et al.* (1992), probability density functions of gas velocity at a particle position are shown in figure 18. The positions of particles in the region $0 < y^+ < 4$ were checked and fluid velocities at those points were examined to construct a p.d.f. The results in figure 18 were calculated by using data from 100 samples well-separated in time. In the figures u is instantaneous streamwise gas velocity at the particle position, $\langle u \rangle$ is the mean value at $y^+ = 4$. Overall particles are found to exist in low-speed regions, with the trend accentuated at low Stokes number. Like the instantaneous fields for glass particles, particles concentrate in low-speed regions in the case of one-way coupling without collision, and the p.d.f. profile is shifted toward the high-speed region in the case of two-way coupling without collision.

4.6. *Particle distribution in the channel-centre region*

Instantaneous particle distributions in the channel centreplane (thickness = 1 mm) are shown in figure 19 for copper, figure 20 for glass and figure 21 for lycopodium. High Stokes number particles tend to disperse uniformly and low Stokes number particles tend to form clouds. The size of the clouds decreases with Stokes number. When inter-particle collision is neglected, low Stokes number particles tend to concentrate in the near-wall region, so that the concentration of lycopodium particle is very low in the channel-centre region.

Figure 22 shows experimental observations by Fessler *et al.* (1994) presented at the same reduced scale as figures 19–21; clouds of lycopodium particles tend to be elongated in the spanwise direction. On the other hand, LES results by Wang & Squires show structures elongated in the streamwise direction as in the near-wall
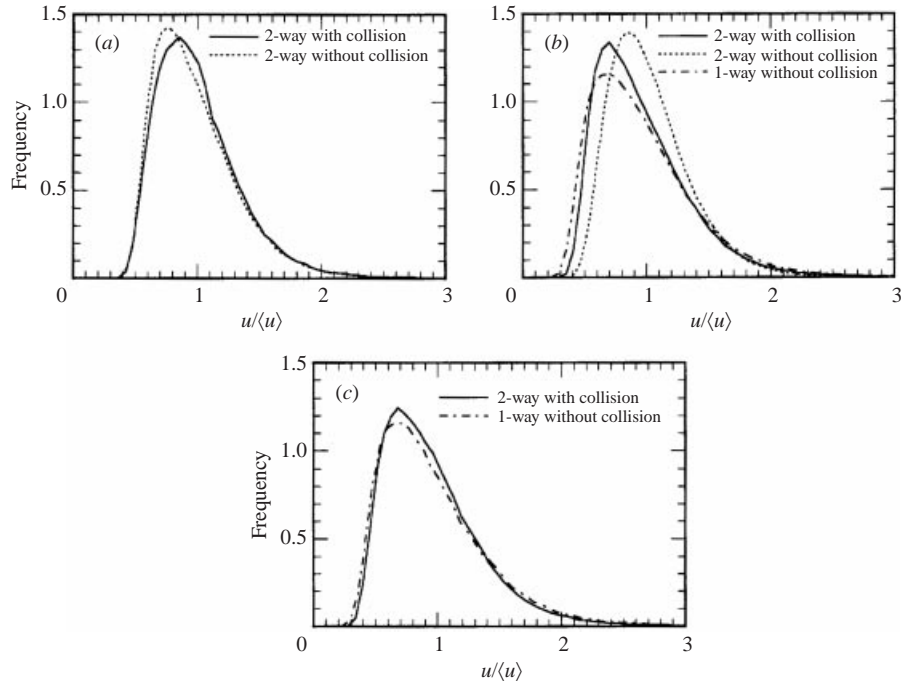
FIGURE 18. Probability density function of fluid velocity at a particle location. u is instantaneous streamwise gas velocity at the particle position, $\langle u \rangle$ is mean value at $y^+ = 4$. (*a*) Copper, $St = 70$, $\phi = 1$; (*b*) glass, $St = 10$; (*c*) lycopodium, $St = 0.89$.
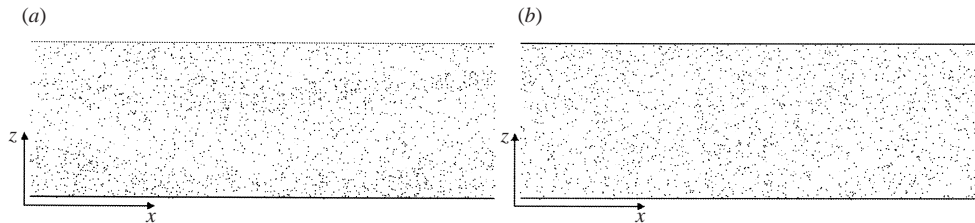

FIGURE 19. Instantaneous particle distribution on the wall-parallel plane in the channel-centre region, copper $St = 70$, $\phi = 1$ (thickness = 1 mm). The size of the area shown is 2880 in the streamwise direction and 960 in the spanwise direction in wall units. (*a*) 2-way without collision, (*b*) 2-way with collision.

region. In the present results considering inter-particle collision, the structure of particle distribution is elongated in the spanwise direction and its scale agrees well with experimental observations by Fessler *et al.* Clouds of glass particles show the same trend as lycopodium, and the present results with inter-particle collisions agree well with experimental observations.

To evaluate the degree of preferential concentration quantitatively, we follow Fessler *et al.* (1994) who examined the deviation of the number density distribution from the Poisson distribution. The Poisson distribution of number density k is given by $e^{-\lambda}\lambda^k/k!$, where λ is the mean number density. When particles are distributed homogeneously, the number density follows the Poisson distribution. On the other hand, when particle clouds are formed, the number density distribution is wider than the Poisson distribution.
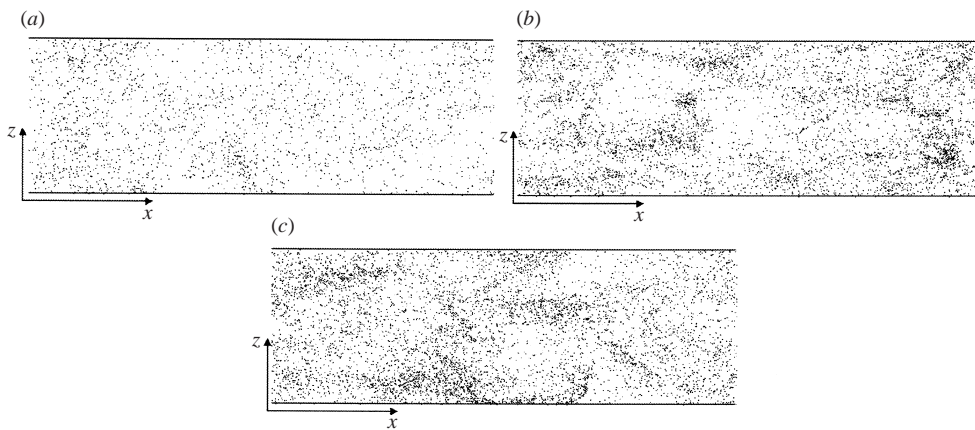
(a)

(b)

(c)

FIGURE 20. As figure 19 but for glass $St = 10$. (a) 1-way without collision,
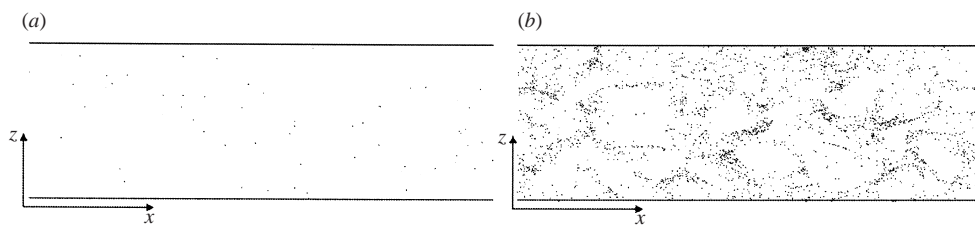(b) 2-way without collision, (c) 2-way with collision.

(a)

(b)

FIGURE 21. As figure 19 but for lycopodium $St = 0.89$. (a) 1-way without collision,
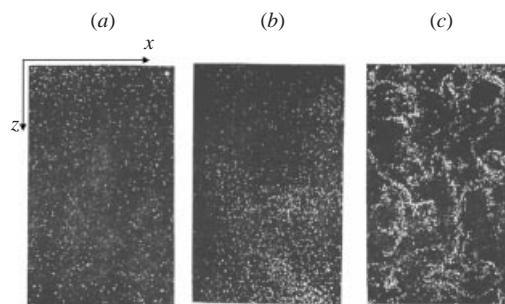(b) 2-way with collision.

(a)   (b)   (c)

FIGURE 22. Experimental observation by Fessler *et al.* (1994) (thickness = 1 mm). The size of the area shown is 966 in the streamwise direction and 1450 in the spanwise direction in wall units. (a) Copper, (b) glass, (c) lycopodium.

A 1 mm thick sheet in the channel centre was subdivided into 2 mm square cells and the number density distribution was calculated in those cells. Figure 23 shows the calculated number density distribution and Poisson distribution for the same number of particles. The horizontal axis k represents the number of particles in a cell and the vertical axis represents the frequency of the particle number density normalized by the total number of cells. The results in figure 23 were calculated by using data from 100 samples well-separated in time.

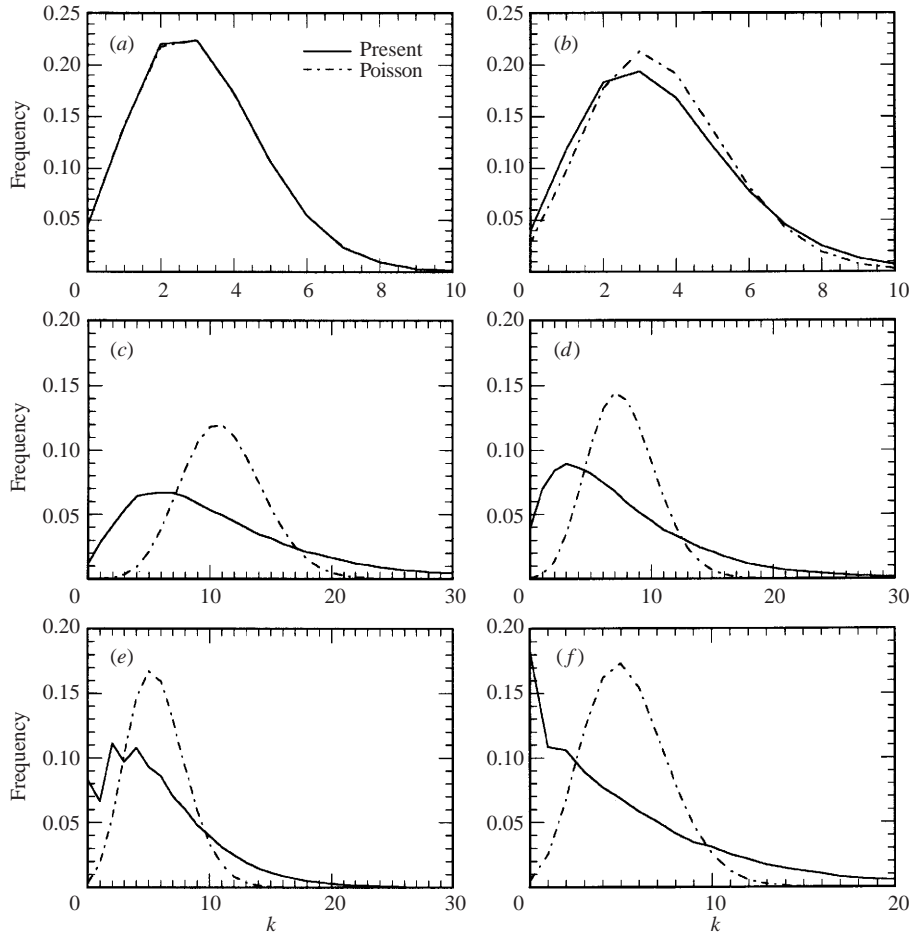For copper, although the effect of inter-particle collision is not obvious in figure

FIGURE 23. Particle number density distribution and Poisson distribution. The horizontal axis k represents the number of particles in a cell and the vertical axis represents the frequency of the particle number density normalized by the total number of cells. (*a*) Copper $\phi = 1$ with collision, (*b*) copper $\phi = 1$ without collision, (*c*) glass 2-way with collision, (*d*) glass 2-way without collision, (*e*) glass 1-way without collision, (*f*) lycopodium 2-way with collision.

19, figures 23(*a*) and 23(*b*) show a difference arising from neglect of inter-particle collisions and suggests that particle clouds would form to a small degree if collisions did not occur. In fact, our results suggest that particles are randomly distributed by diffusion due to inter-particle collisions. The results for glass particle are shown in figure 23(*c–e*) for different computational cases. The Poisson distribution in each case differs according to the mean number density in the channel-centre region. Deviations from the Poisson distribution, suggesting particle clouds, are similar in each case. For lycopodium particles (figure 23*f*), the distribution function is considerably widened by formation of particle clouds.

This evaluation method depends on the cell size for calculating number density. Fessler *et al.* (1994) evaluated the degree of preferential concentration in particle clouds for various cell sizes by the parameter D:

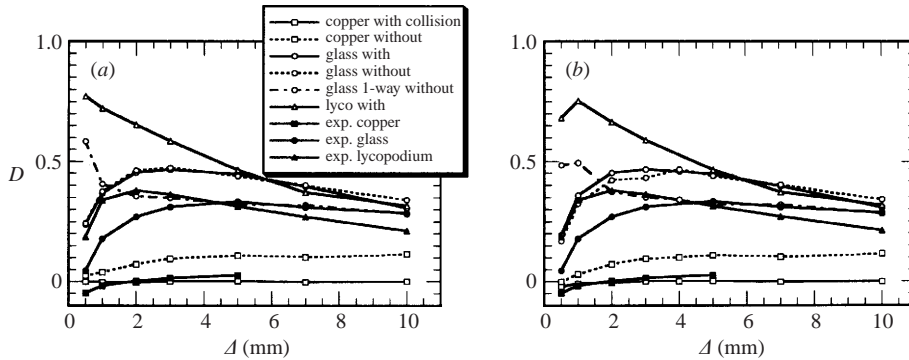$$D = (\sigma - \sigma_{pois})/\lambda, \tag{4.1}$$

FIGURE 24. Normalized deviation D of the standard deviation of particle frequency distribution from Poisson distribution as a function of cell size (equation (4.1)), with experimental results by Fessler *et al.* (1994): (*a*) by raw data, (*b*) with identification of overlapped particles within 0.1 mm as one particle.

where σ and σ_{pois} are the standard deviations for the calculated number density distribution and Poisson distribution, respectively. For cells much larger than a particle cloud, or for very small cells which scarcely contain any particles, the particle distribution is effectively random and the number density distribution approaches the Poisson distribution. Thus, D reaches a maximum when the cell size matches the size of particle clouds (Fessler *et al.* 1994). Figure 24(*a*) shows the change of D for varying cell size Δ.

For copper, results accounting for collision show $D \simeq 0$ at any cell size so that particles are distributed randomly. The experimental result by Fessler *et al.* (1994) also shows $D \simeq 0$. In the case without inter-particle collision, D increases with cell size.

For glass particles with two-way coupling, no effect of inter-particle collision on D is apparent. For small Δ, D increases with Δ, and then decreases for large Δ, in agreement with the experimental trend. Quantitatively D is larger in the computational results than experimentally, and Δ at maximum D is about 5 mm in the present result and about 3 mm in the experiment. In the case of glass with one-way coupling, the profile is qualitatively different from experimental results, i.e. D simply decreases with increasing Δ.

For lycopodium, D is monotonically decreasing with Δ, in contrast to experimental results as well as glass with one-way coupling. This discrepancy is inconsistent with the good agreement in the characteristics of particle clouds between figures 21 and 22. The cause of this discrepancy is not obvious; however there is a possibility that overlap of particle images caused such errors in the experimental image processing. So, D is re-evaluated by regarding particles separated by a small distance when viewed along the *y*-axis as one particle. Figure 24(*b*) shows the revised relation between D and Δ, taking particles overlapped within 0.1 mm as one particle. The revised profile approaches the experimental one.

Although the thickness of the sheet was varied in the range from 0.5 mm to 5 mm, the trends are almost the same as those of figures 23 and 24 for 1 mm.

4.7. *Stokes number based on mean free time of collision*

In the above investigation, the trend of preferential concentration with the difference of Stokes number based on large-eddy time scale was shown. In this section, the
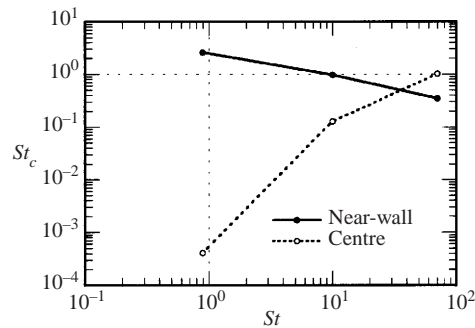
FIGURE 25. Relation between Stokes number St based on the time scale of large eddy and St_c based on the mean free time of collision.

effect of inter-particle collision on the preferential concentration is discussed using the Stokes number based on the mean free time of collision. The Stokes number based on particle relaxation time and the mean free time of collision is defined as

$$St_c = (\tau_p)/\tau_{mf}. \tag{4.2}$$

If $St_c \ll 1$ then the flow is dilute, that is, the particles have sufficient time to respond to changes in the fluid velocity. On the other hand, if $St_c \gg 1$, then the collisions control particle motion and the flow is dense. In this section, the Stokes number in the near-wall region and in the channel-centre region were evaluated separately because flow patterns in those regions are completely different. Figure 25 shows the correlation between Stokes numbers based on the time scale of the large eddy and on the mean free time of collision. The mean free time was calculated by counting the number of collision during one period of a simulation.

In the near-wall region, St_c decreases as St increases, that is, the effect of inter-particle collision is larger on the particles that greatly depend on turbulent eddies. This is because small-scale eddies in the near-wall region have large energy and make particles collide. Thus, when preferential concentration occurs by turbulence, the effect of inter-particle collision on the structure of particle distribution cannot be negligible.

In the channel-centre region, St_c increases with St, that is, the effect of inter-particle collision is larger on the particles that move independently of turbulent eddies. This is because small-scale eddies in the channel-centre region do not have large energy and large-scale eddies, which can give particles energy, control the phenomena. In this case, inter-particle collisions cannot affect the preferential concentration by turbulence.

Note that, however, this discussion is limited to the flows in the wall-parallel planes and that the structures in these planes are formed by the effect of inter-particle collision on the transverse particle dispersion. The discussion in this section does not contradict previous sections and shows that the effect of inter-particle collision on the preferential concentration is determined by Stokes number based on the mean free time of collision.

5. Summary

Simulations of gas–solid turbulent flow in a vertical downward channel flow at $Re_\tau = 644$ were performed in order to study the interaction between particle motion and gas turbulence and to clarify the effect of inter-particle collision. Also, the minimum length scale of eddies which affect the particle motion was related to

Stokes number, and the spatial resolution required in LES of two-phase flow was investigated.

It was found that inter-particle collision encourages transverse mixing and the effect of the mixing flattens the profiles of particle velocity and particle concentration even in very dilute conditions (solid volume fraction $O(10^{-4})$). Numerical results of particle fluctuation velocity by considering inter-particle collision approach experimental results much better than results without collision. As a result, inter-particle collision cannot be disregarded at such a concentration.

Concerning turbulence modification, numerical results were able to reproduce the trends only for small Stokes number.

The spatial structure of instantaneous flow fields was visualized. It was found that particle clouds were formed by the effect of turbulence structure (so called 'preferential concentration') at small Stokes number particles if inter-particle collision was ignored. Once particle clouds were formed, results were different for one-way coupling and two-way coupling because turbulence structure is affected by particle clouds. Inter-particle collisions disperse particles in the transverse direction so that the structure of particle distribution in wall-parallel planes with and without collisions are greatly different, in particular in the near-wall region. The shape and scale of particle clouds observed in the channel-centre region by considering inter-particle collision agreed well with experimental observation, unlike LES results by Wang & Squires. Thus inter-particle collision greatly affects preferential concentration.

The effect of inter-particle collision on the preferential concentration in the wall-parallel plane is determined by Stokes number based on the mean free time of collision and on the time scale of fluid turbulence. In the near-wall region, inter-particle collisions affect the motion of large-inertia particles and in the channel-centre region affect the motion of small-inertia particles.

REFERENCES

BIRD, G. A. 1976 *Molecular Gas Dynamics*. Clarendon.

DAVIES, J. M. 1949 The aerodynamics of golf balls. *J. Appl. Phys.* **20**, 821–828.

DEARDORFF, J. W. 1970 A numerical study of three-dimensional turbulent channel flow at large Reynolds numbers. *J. Fluid Mech.* **42**, 453–480.

DENNIS, S. C. R., SINGH, S. N. & INGHAM, D. B. 1980 The steady flow due to a rotating sphere at low and moderate Reynolds numbers. *J. Fluid Mech.* **101**, 257–279.

ELGHOBASHI, S. & TRUESDELL, G. C. 1992 Direct simulation of particle dispersion in a decaying isotropic turbulence. *J. Fluid Mech.* **242**, 655–700.

ELGHOBASHI, S. & TRUESDELL, G. C. 1993 On the two-way interaction between homogeneous turbulence and dispersed solid particles. I: Turbulence modification. *Phys. Fluids* A **5**, 1790–1801.

FESSLER, J. R., KULICK, J. D. & EATON, J. K. 1994 Preferential concentration of heavy particles in a turbulent channel flow. *Phys. Fluids* **6**, 3742–3749.

GERMANO, M., PIOMELLI, U., MOIN, P. & CABOT, W. H. 1991 A dynamic subgrid-scale eddy viscosity model. *Phys. Fluids* A **3**, 1760–1765.

GORE, R. A. & CROWE, C. T. 1991 Modulation of turbulence by a dispersed phase. *Trans. ASME: J. Fluids Engng* **113**, 304–307.

HALL, D. 1988 Measurements of the mean force on a particle near a boundary in turbulent flow. *J. Fluid Mech.* **187**, 451–466.

KAFTORI, D., HETSRONI, G. & BANERJEE, S. 1995a Particle behavior in the turbulent boundary layer I. motion, deposition, and entrainment. *Phys. Fluids* **7**, 1095–1106.

KAFTORI, D., HETSRONI, G. & BANERJEE, S. 1995b Particle behavior in the turbulent boundary layer II. velocity and distribution profiles. *Phys. Fluids* **7**, 1107–1121.

KAJISHIMA, T. & MIYAKE, Y. 1990 Estimation of turbulence models by large eddy simulation with high-resolution grids. *JSME Intl J.* II, **33**-1, 73–79.

KULICK, J. D., FESSLER, J. R. & EATON, J. K. 1994 Particle response and turbulence modification in fully developed channel flow. *J. Fluid Mech.* **277**, 109–134.

MACCOLL, J. H. 1928 Aerodynamics of a spinning sphere. *J. R. Aero. Soc.* **32**, 777–798.

MAXEY, M. R. & RILEY, J. J. 1983 Equation of motion for a small rigid sphere in nonuniform flow. *Phys. Fluids* **26**, 883–889.

MOIN, P. & KIM, J. 1982 Numerical investigation of turbulent channel flow. *J. Fluid Mech.* **118**, 341–377.

PAN, Y. & BANERJEE, S. 1996 Numerical simulation of particle interaction with wall turbulence. *Phys. Fluids* **8**, 2733–2755.

PAN, Y. & BANERJEE, S. 1997 Numerical investigation of the effects of large particles on wall-turbulence. *Phys. Fluids* **9**, 3786–3807.

PEDINOTTI, S., MARIOTTI, G. & BANERJEE, S. 1992 Direct numerical simulation of particle behaviour in the wall region of turbulent flows in horizontal channels. *Intl J. Multiphase Flow* **18**, 927–941.

RASHIDI, M. HETSRONI, G. & BANERJEE, S. 1990 Particle-turbulence interaction in a boundary laryer. *Intl J. Multiphase Flow* **16**, 935–949.

ROUSON, D. W. I. & EATON, J. K. 1994 Direct numerical simulation of turbulent channel flow with immersed particles. In *Numerical Methods in Multiphase Flows*. FED-Vol. 185, pp. 47–57. ASME.

SAFFMAN, P. G. 1965 The lift on a small sphere in a slow shear flow. *J. Fluid Mech.* **22**, 385–400.

SCHILLER, L. & NAUMAN, A. 1933 *Z. Ver. Dtsch. Ing.* **77**, 318–320.

SIMONIN, O. 1991 Prediction of the dispersed phase turbulence in particle-laden jets. In *Gas–Solid Flows*. FED-Vol. 121, pp. 197–206. ASME.

SOMMERFELD, M. 1995 The importance of inter-particle collisions in horizontal gas-solid channel flows. In *Gas-Particle Flows*. FED-Vol. 228, pp. 335–345. ASME.

SQUIRES, D. K. & EATON, J. K. 1990 Particle response and turbulence modification in isotropic turbulence. *Phys. Fluids* A **2**, 1191–1203.

SUNDARAM, S. & COLLINS, L. R. 1997 Collision statistics in an isotropic particle-laden turbulent suspension I. direct numerical simulations. *J. Fluid Mech.* **335**, 75–109.

SUNDARAM, S. & COLLINS, L. R. 1999 A numerical study of the modulation of isotropic turbulence by suspended particles. *J. Fluid Mech.* **379**, 105–143.

TAKAGI, H. 1977 Viscous flow induced by slow rotation of a sphere. *J. Phys. Soc. Japan* **42**, 319–325.

TANAKA, T. & TSUJI, Y. 1991 Numerical simulation of gas-solid two-phase flow in a vertical pipe: On the effect of inter-particle collision. In *Gas-Solid Flows*. FED-Vol. 121, pp. 123–128. ASME.

WANG, L. P., WEXLER, A. S. & ZHOU, Y. 1998a On the collision rate of small particles in isotropic turbulence I. zero-inertia case. *Phys. Fluids* **10**, 266–276.

WANG, L. P., WEXLER, A. S. & ZHOU, Y. 1998b On the collision rate of small particles in isotropic turbulence II. finite inertia case. *Phys. Fluids* **10**, 1206–1216.

WANG, Q. & SQUIRES, K. D. 1996 Large eddy simulation of particle-laden turbulent channel flow. *Phys. Fluids* **8**, 1207–1223.

WANG, Q., SQUIRES, K. D., CHEN, M. & MCLAUGHLIN, J. B. 1997 On the role of the lift force in turbulence simulations of particle deposition. *Intl J. Multiphase Flow* **23**, 749–763.

YONEMURA, S., TANAKA, T., & TSUJI, Y. 1993 Cluster formation in gas-solid flow predicted by the DSMC method. In *Gas-Solid Flows*. FED-Vol. 166, pp. 303–309. ASME.